Hydrodynamic Instabilities from the Beginning to the End

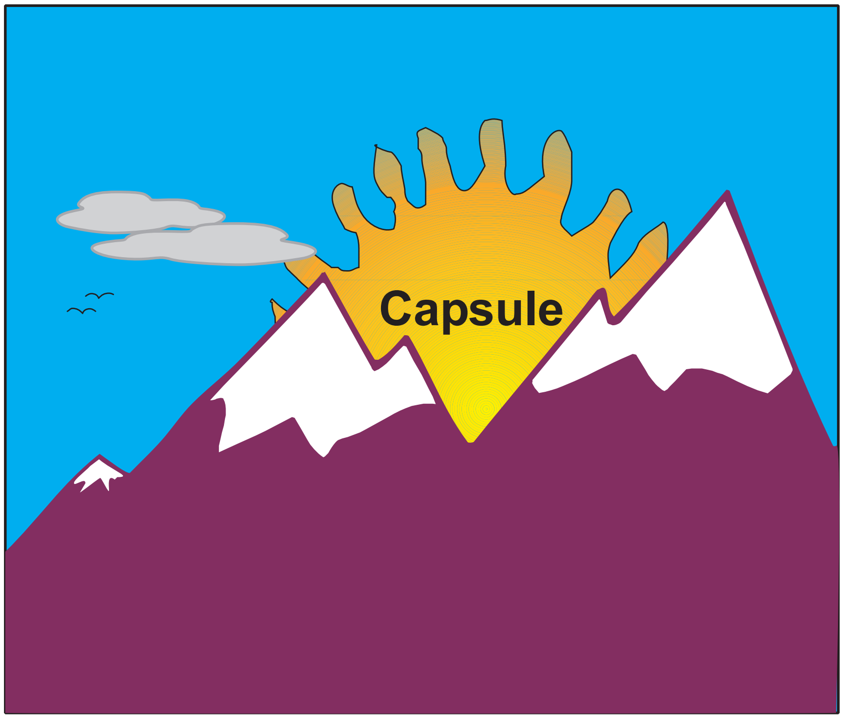

Implosion at dawn

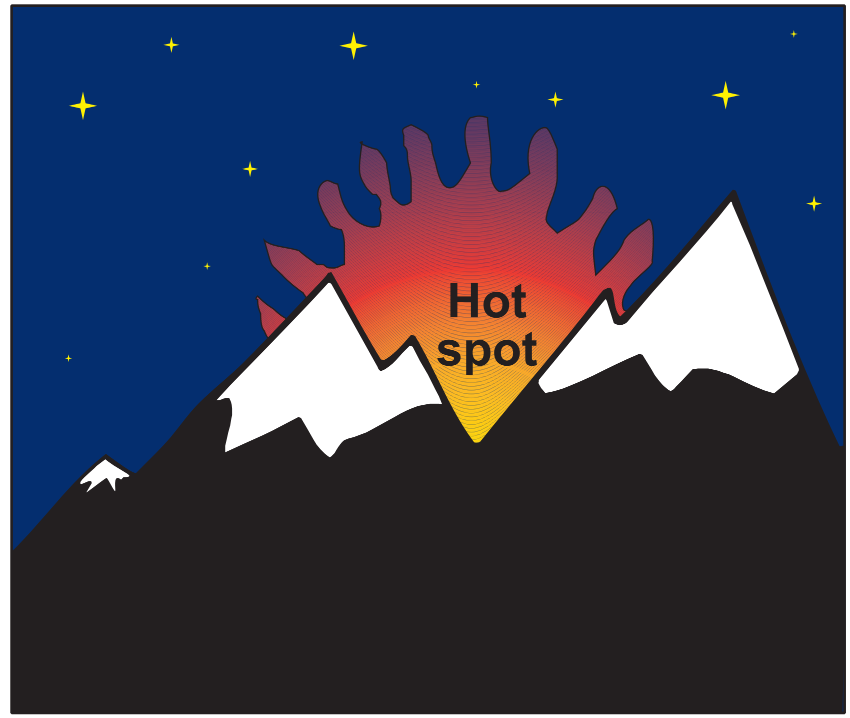

Implosion at sunset

R. Betti, V. Goncharov, J. Knauer,
V. Lobatchev, and M. Umanski
University of Rochester
Laboratory for Laser Energetics

30th Annual Anomalous
Absorption Conference
Ocean City, MD
21–26 May 2000

Acceleration or deceleration, this is the question!

Shock transit and acceleration phase

- RM and RT growth
- RT and RM seeding:
  - outer-surface nonuniformities
  - inner-surface nonuniformities (feedout)
  - laser imprintings

Reflected shock transit and deceleration phase

- RM and RT growth
- RT and RM seeding:
  - outer-surface nonuniformities (feedout)
  - inner-surface nonuniformities (feedthrough)

Why all this theory is so incredibly useful!

Why all this theory is so incredibly useful!

UR LLE

- Keeps theorists employed.
- Improves physical understanding.
- Provides feedback to numerical simulations.
- Leads to the development of a fast, reliable, and accurate postprocessor of 1-D codes. Target design can be carried out using such a postprocessor and subsequently refined using 2-D simulations.

Acceleration Phase

The classical RT is just Newton's law at work: F = ma!

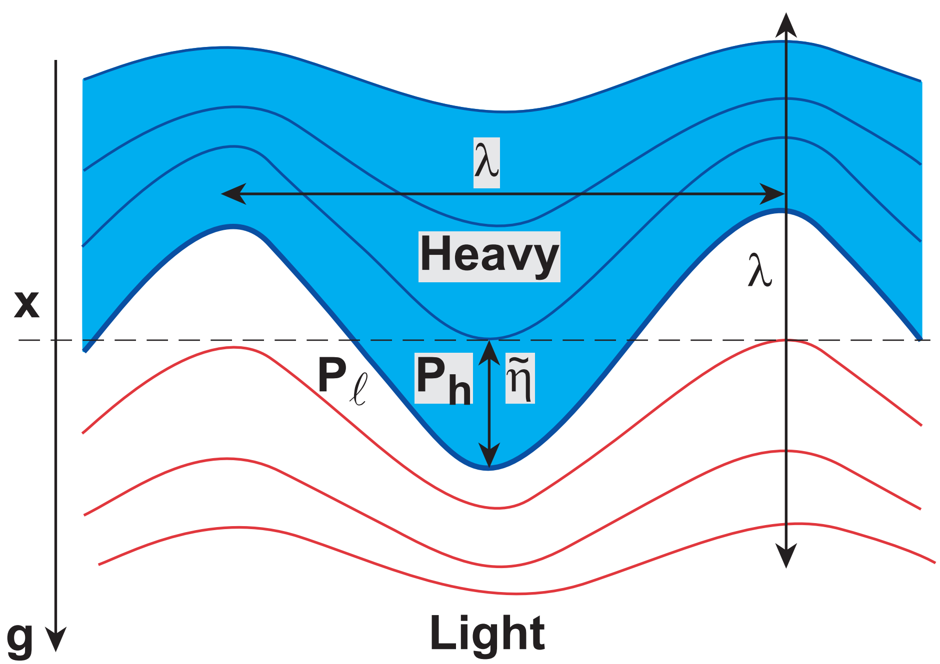

$$F = S(P_h - P_\ell) = ma = \rho_h \lambda S \ddot{\tilde{\eta}}$$

$$\frac{dP_0}{dx} = \rho_0 g = \begin{cases} \rho_h g & \text{heavy} \\ \rho_\ell g & \text{light} \end{cases}$$

$$P_\ell = P_0 + \left[\frac{dP_0}{dx}\right]_\ell \tilde{\eta} = P_0 + \cancel{\rho_\ell g \tilde{\eta}}$$

$$P_h = P_0 + \left[\frac{dP_0}{dx}\right]_h \tilde{\eta} = P_0 + \rho_h g \tilde{\eta}$$

$$F = ma \rightarrow S\rho_h g\tilde{\eta} = \rho_h \lambda S \ddot{\tilde{\eta}} \rightarrow \ddot{\tilde{\eta}} = kg\tilde{\eta} \rightarrow \tilde{\eta} \sim e^{\gamma t} \rightarrow \gamma = \sqrt{kg}$$

$k \sim 1/\lambda$

TC5382

Acceleration Phase

The ABLATIVE RT is just Newton's law at work again but with a restoring force: the dynamic pressure

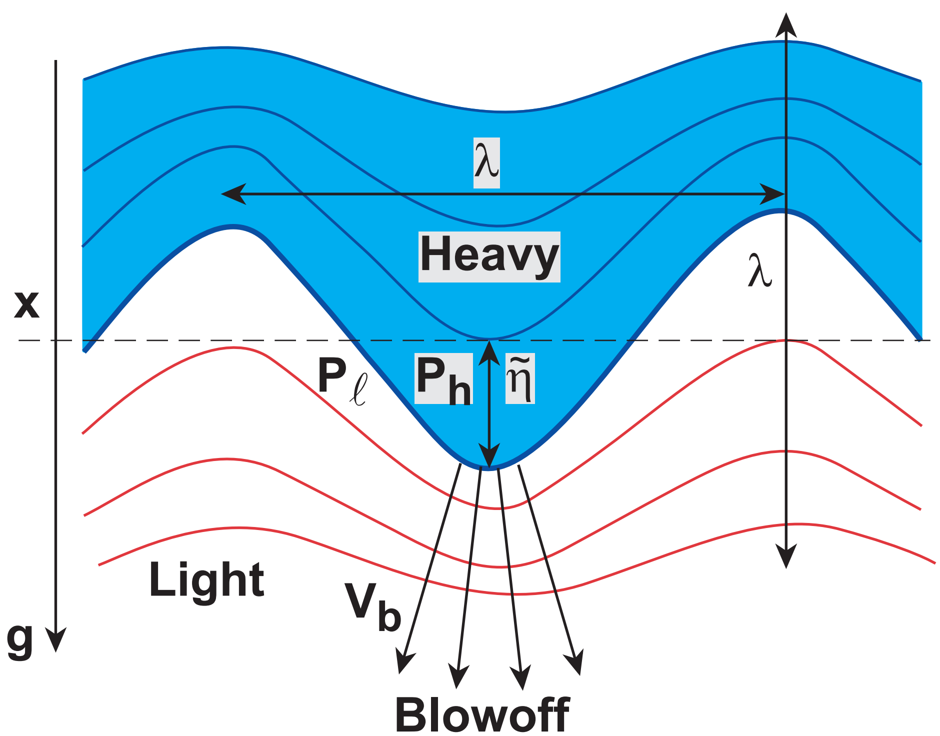

- **Newton's law**

$$S[P_h - (P_\ell + \rho_\ell V_b^2)] = \rho_h \lambda S \ddot{\tilde{\eta}}$$

- **Energy balance**

$$pV_b = q_{heat} \rightarrow \tilde{V}_b = V_b \tilde{\eta}/\lambda$$

- **Perturbed dynamic pressure**

$$\underbrace{\rho_\ell V_b}_{\text{Ablation rate}} \tilde{V}_b = \dot{m} V_b \tilde{\eta}/\lambda$$

Restoring force

Stabilizing

- **Growth rate:** $S(\rho_h g - k\dot{m}V_b)\tilde{\eta} = \rho_h \lambda S \ddot{\tilde{\eta}} \rightarrow \tilde{\eta} \sim e^{\gamma t} \rightarrow \gamma = \sqrt{kg - k^2 \frac{\dot{m}}{\rho_h} V_b}$

TC5383

Acceleration Phase

The "old"-fashioned ablative stablization is still there but it is not very effective

- A more accurate calculation yields additional stablization:

$$\gamma = \sqrt{Akg - k^2 \frac{\dot{m}}{\rho_h} V_b + 4k^2 V_a^2} - 2kV_a$$

"Old"-fashioned

Dynamic pressure

- Atwood number: $A = \dfrac{\rho_{heavy} - \rho_{light}(\lambda)}{\rho_{heavy} + \rho_{light}(\lambda)} \approx 1$

- The cutoff wave number depends only on the dynamic pressure:

$$kg = k^2 \frac{\dot{m}}{A\rho_h} V_b \rightarrow k_{cutoff} = \frac{\rho_h g}{\dot{m} V_b A}$$

J. Sanz, Phys. Rev. E 53, 4026 (1996); R. Betti, V. Goncharov *et al.*, Phys. Plasmas 5, 1446 (1996).

TC5384

The ABLATIVE RM is NOT an instability but just damped oscillations

Impulsive acceleration

- Newton's law: $[\rho_h g(t) - k\dot{m}V_b]\,\tilde{\eta} = \rho_h \lambda \ddot{\tilde{\eta}}$ $\qquad g(t) = U_{shell}\,\delta(t)$

- For $t = 0^+$, $\dot{\tilde{\eta}}(0)^+ = kU_{shell}\tilde{\eta}(0)$ $\qquad \boxed{\omega = \sqrt{k^2 \frac{\dot{m}}{\rho_h} V_b}}$

- For $t > 0^+$, $g(t) = 0 \;\rightarrow\; \tilde{\eta}(t) = \tilde{\eta}(0)^+ \cos(\omega t) + \frac{\dot{\tilde{\eta}}(0)^+}{\omega}\sin(\omega t)$

- If the ablative convection of vorticity is included then the RM is damped:

$$\tilde{\eta}(t) = \left\{\tilde{\eta}(0)\cos(\omega t) + \frac{\dot{\tilde{\eta}}(0) + 2kV_a\tilde{\eta}(0)}{\omega}\sin(\omega t)\right\} e^{-2kV_a t}$$

A. Velikovich *et al.*, Phys. Plasmas 5, 1491 (1998); V. Goncharov, Phys. Rev. Lett. 82, 2091 (1999).

Prediction of the sharp boundary model agrees with the numerical results

200 μm-thick DT ice, 100 TW/cm^2 square laser pulse, λ = 20 μm, $\tilde{\eta}_0$ = 0.1 μm

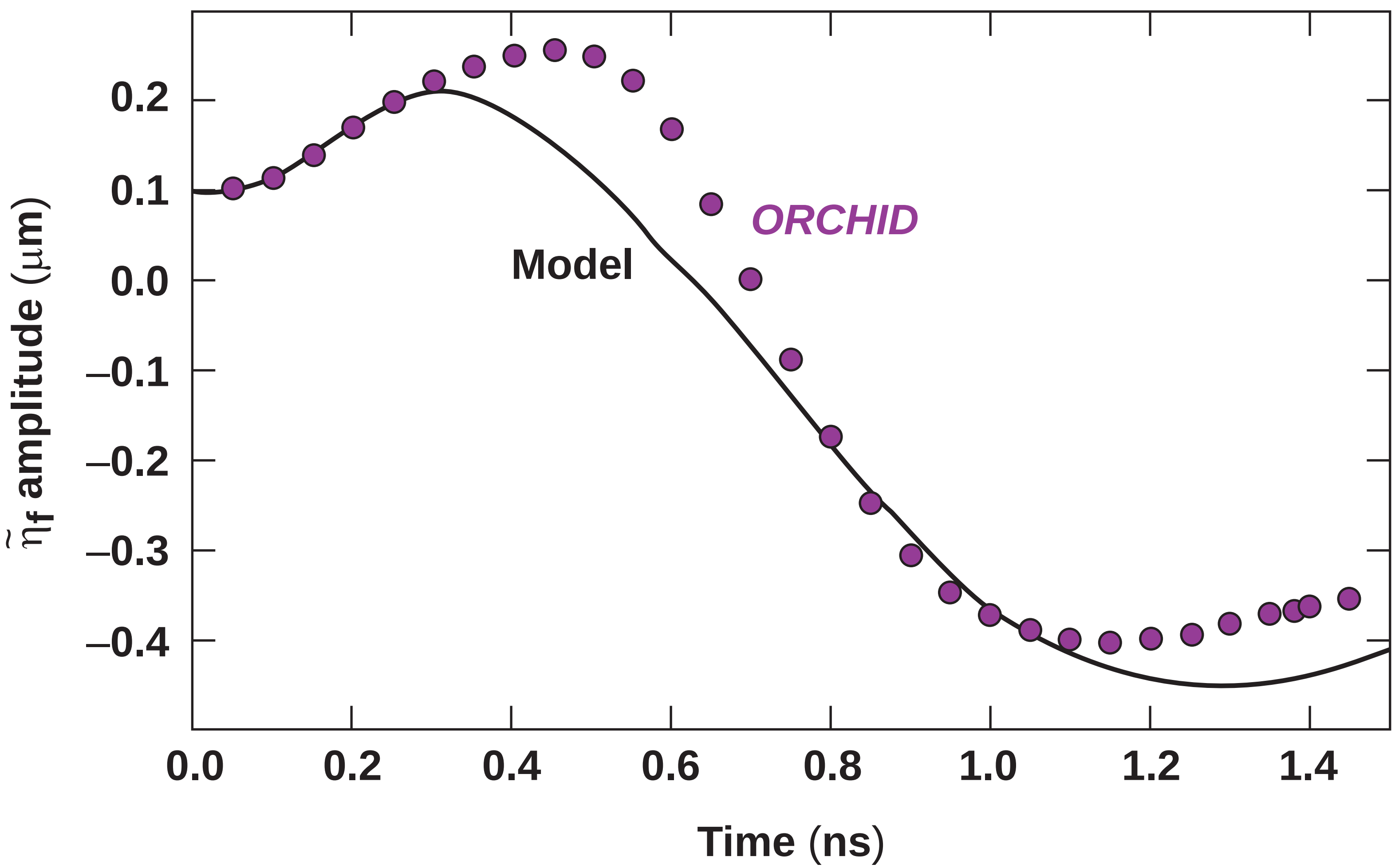

TC4840

The RT postprocessor is based on the sharp boundary model

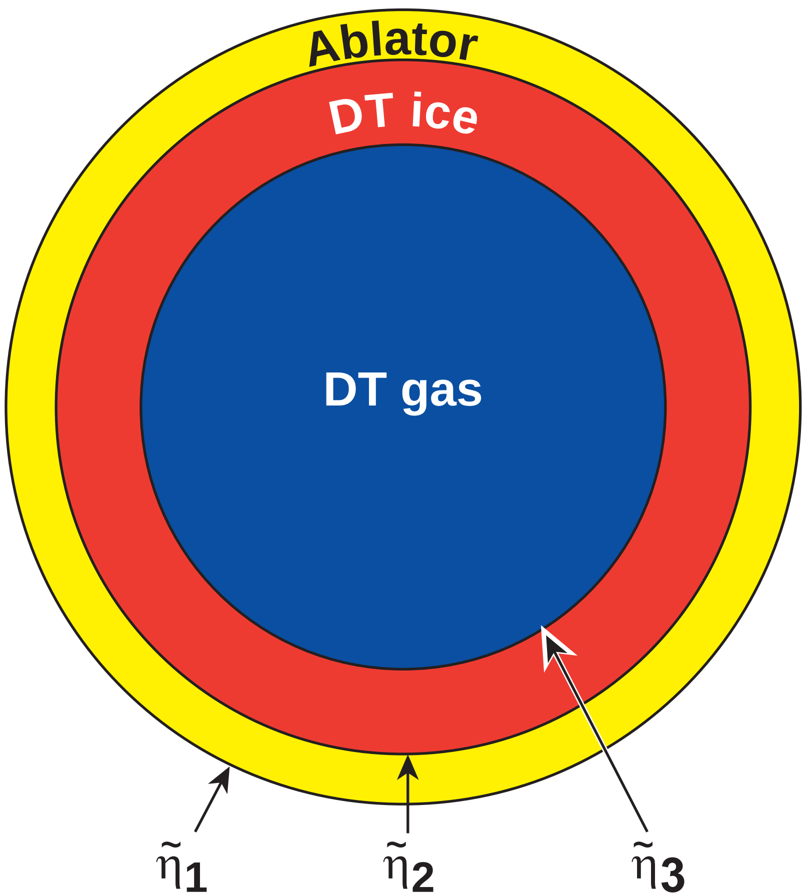

- $\tilde{\eta}$ represents the surface distortion.
- The model is based on a set of coupled second-order differential equations:

$$\sum_{j=1}^{N} a_j(t)\ddot{\tilde{\eta}}_j + b_j(t)\dot{\tilde{\eta}}_j + c_j(t)\tilde{\eta}_j = 0$$

- Physics included
  - thermal conduction
  - ablative flow
  - compressibility
- The soulution of the model requires the initial conditions: $\eta_j(0)$, $\dot{\eta}_j(0)$

- All the details of sharp boundary model can be found in V. Goncharov's PhD thesis (UR 1998).

TC5386

RT seeding by rear-surface nonuniformities

Feedout

After the shock breaks out, a rarefaction wave propagates toward the ablation front while the rear surface expands; after the rarefaction wave breaks out, the ablation front accelerates

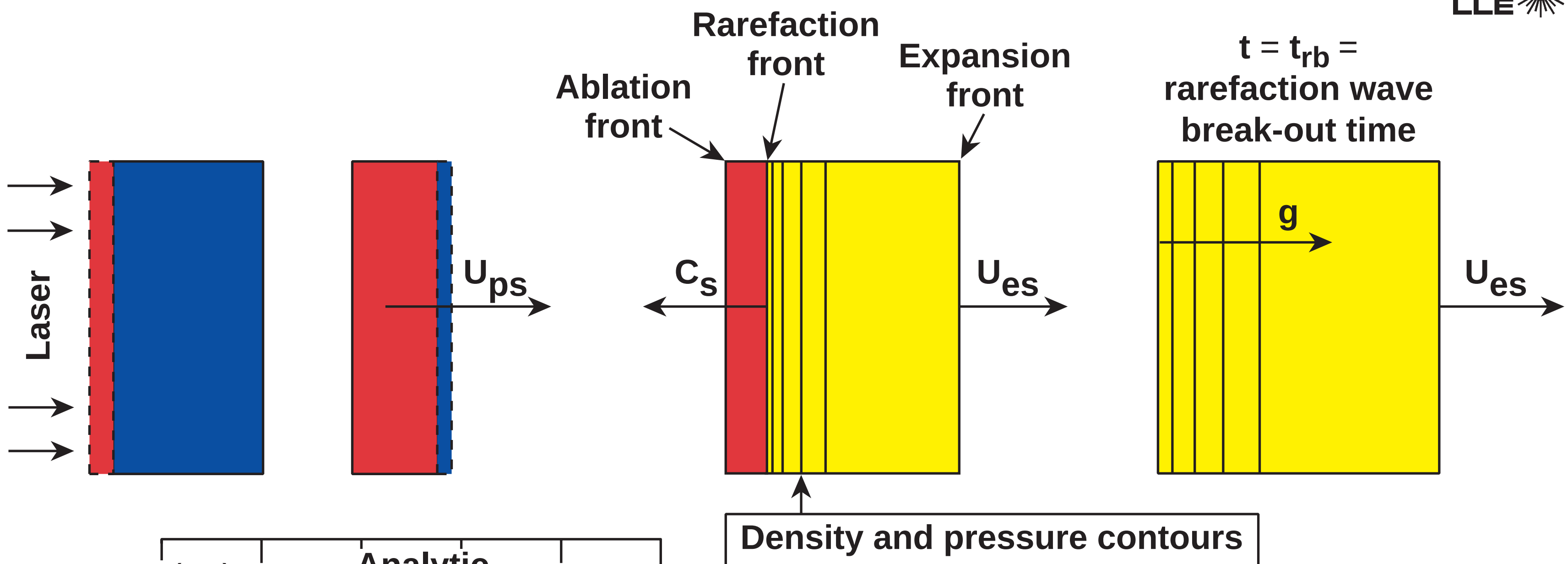

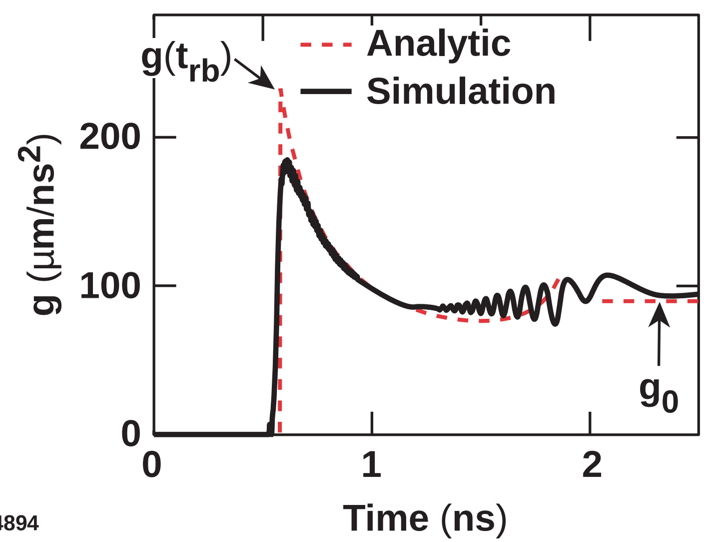

$$g(t_{rb}) = 2.5\, g_0$$

$$g_0 \equiv g(\text{steady state}) = \frac{P_a}{\rho d}$$

TC4894

For the analytic solution, see R. Betti *et al.* (PRL, 1998)

Two-dimensional behavior in the presence of a rippled rear surface

(a) The shock reaches the rippled rear surface.

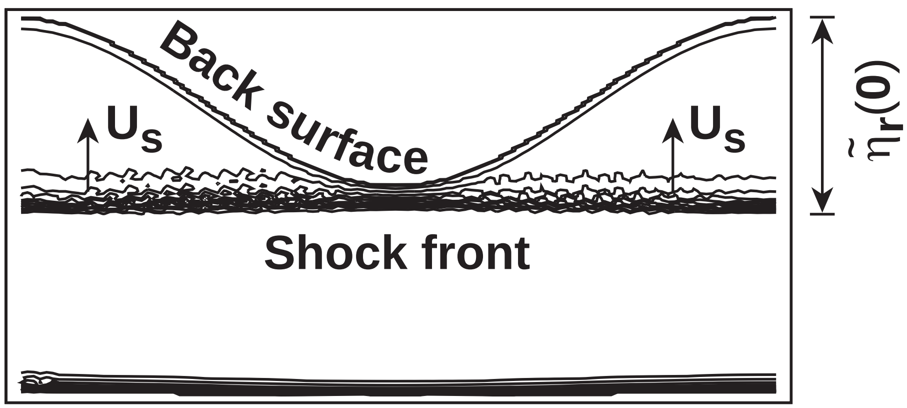

(b) Shock and rippled surface interact.

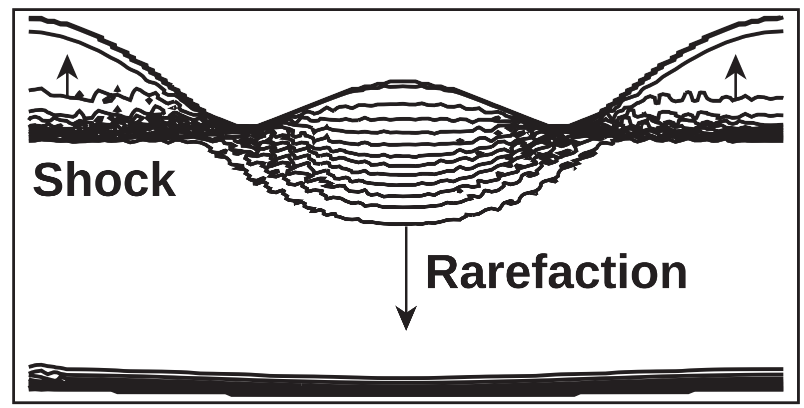

(c) The rippled rarefaction front is formed.

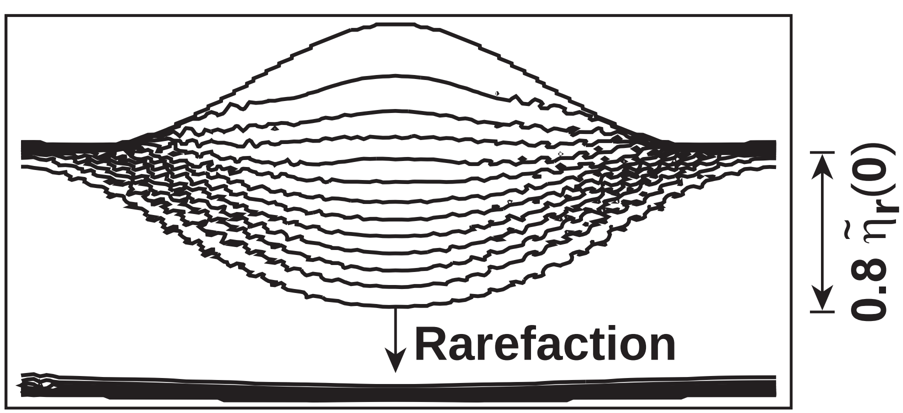

(d) The rarefaction reaches the front surface.

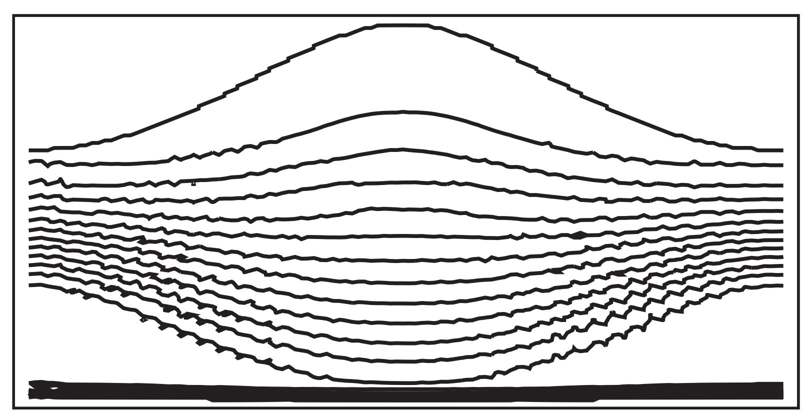

TC4882

After the rarefaction breakout the ripple on the front surface is seeded and begins to grow

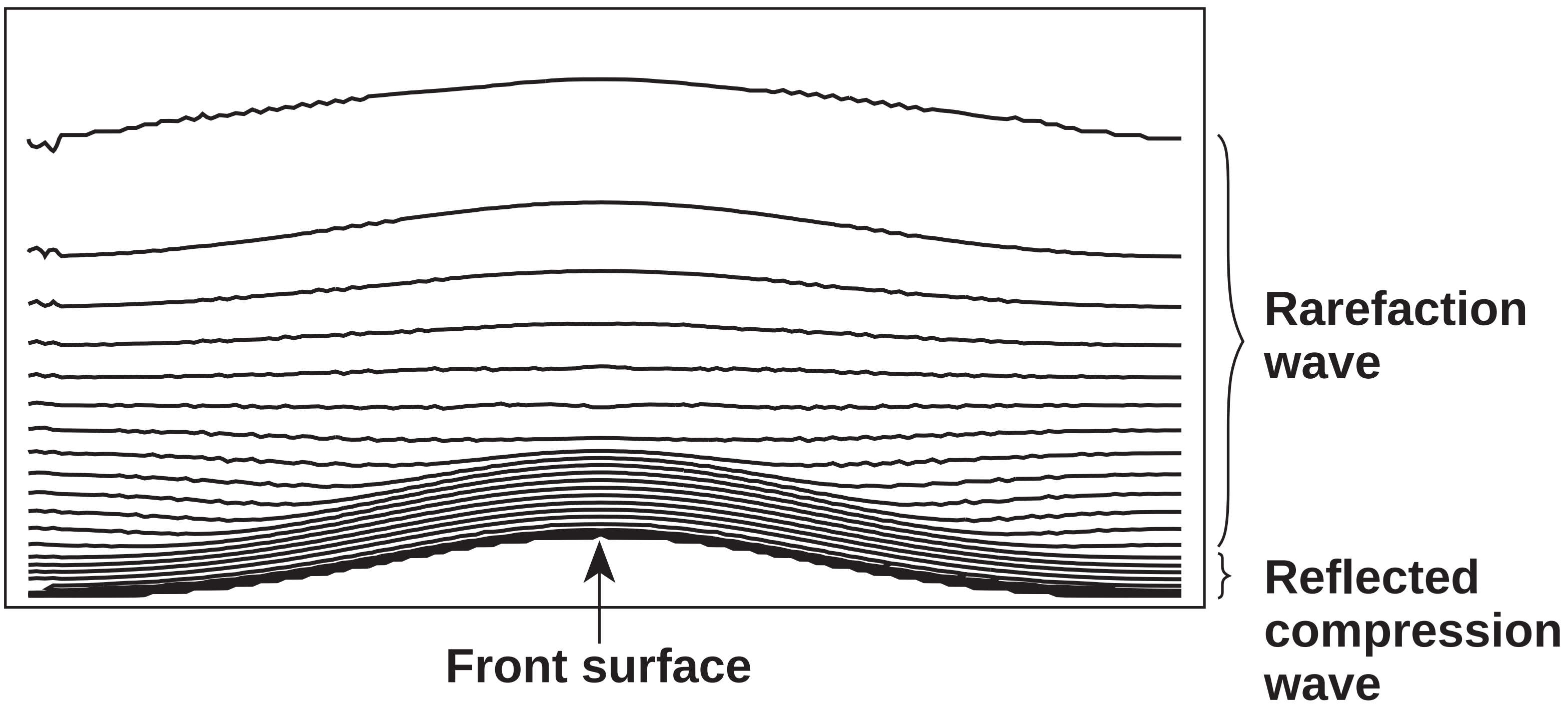

0.1 ns after rarefaction breakout

When the rippled rarefaction wave reaches the ablation front, it imprints a velocity perturbation and the ablation front develops a ripple that starts growing linearly in time

UR LLE

$t = t_{rb}$ = rarefaction-wave break-out time

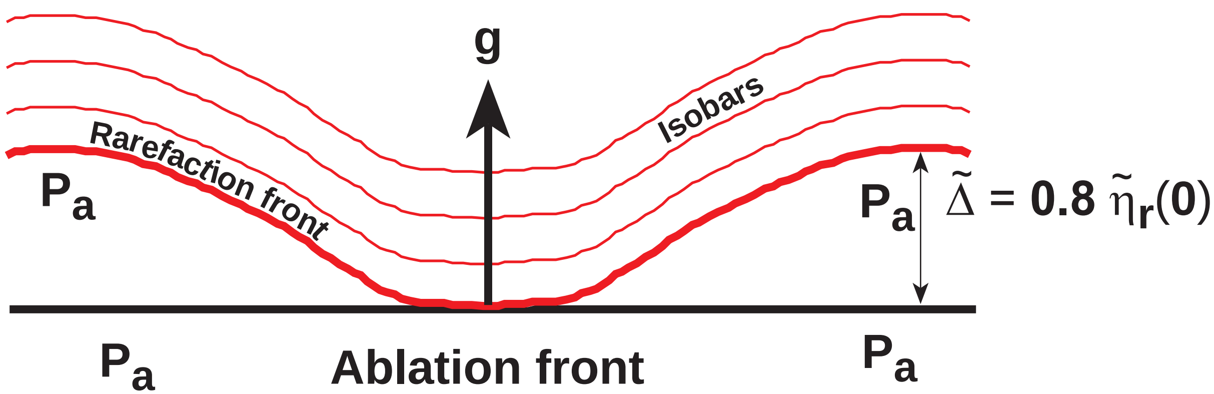

$$\Delta t = \frac{\tilde{\Delta}}{C_s}$$

$$g(t_{rb}) = \frac{5}{2}\frac{P_a}{\rho d}$$

$t = t_{rb} + \Delta t$

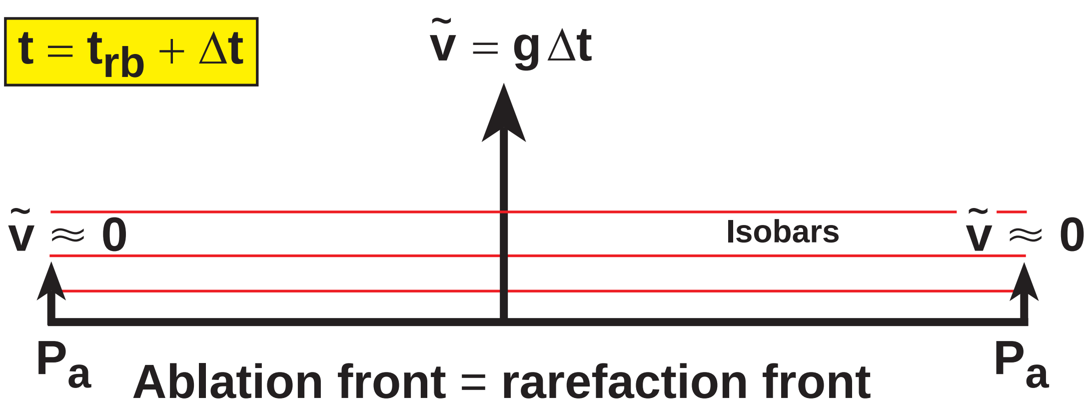

$$\tilde{v} = g\Delta t$$

$$\tilde{v} = \frac{6}{5} C_s \frac{\tilde{\eta}_r(0)}{d_{comp}}$$

→ This theory is valid only for $kd_{comp} < 1$.

TC4690

The predicted ablation-front-surface ripple-amplitude evolution soon after the rarefaction wave breaks out does NOT accurately reproduce the simulation results

Ablation-front-surface distortion versus time

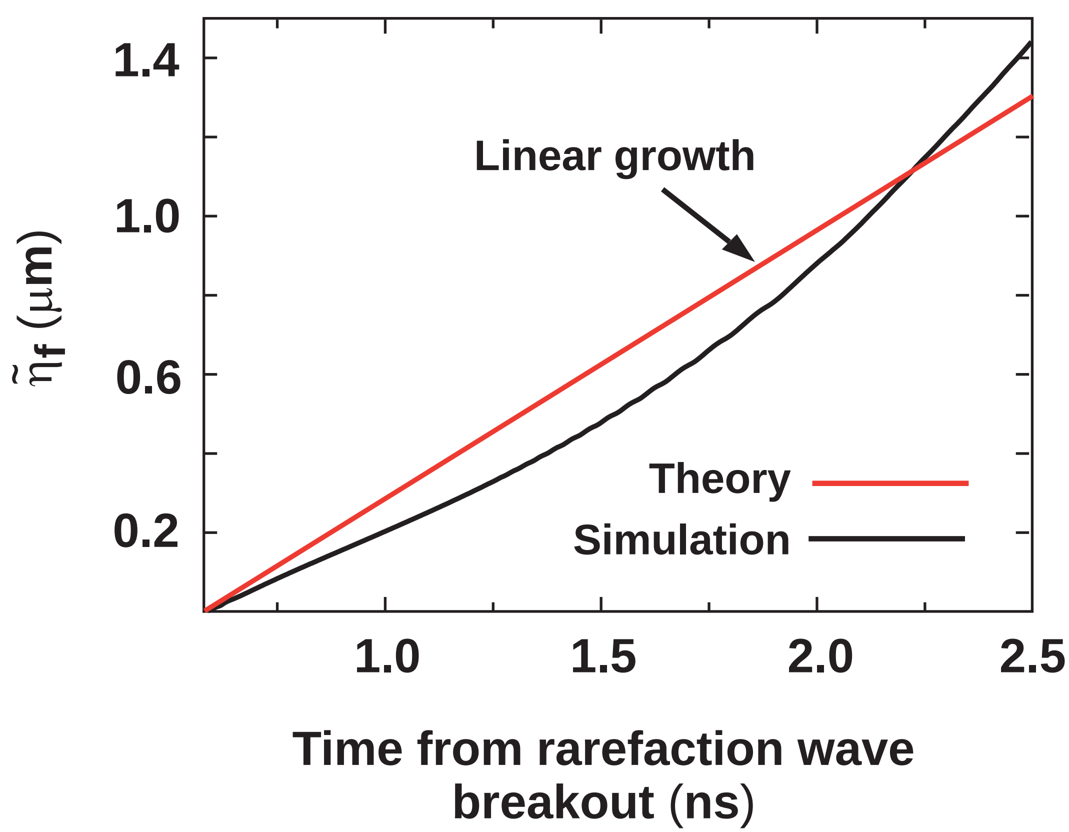

The theory predicts a linear growth right after the rarefaction wave breaks out.

$\tilde{\eta}_f = \tilde{v}\, t$

$\tilde{\eta}_r(0) = 0.1\ \mu m$

$\tilde{v} \approx 0.7\ \mu m/ns$

$k\, d_{comp} = 0.033$

$P = 20$ Mbar

$d\ (CH) = 20\ \mu m$

$d_{comp} \simeq d/4$

TC4695

In addition to the linear growth, an approximately quadratic growth occurs because of the perturbed acceleration

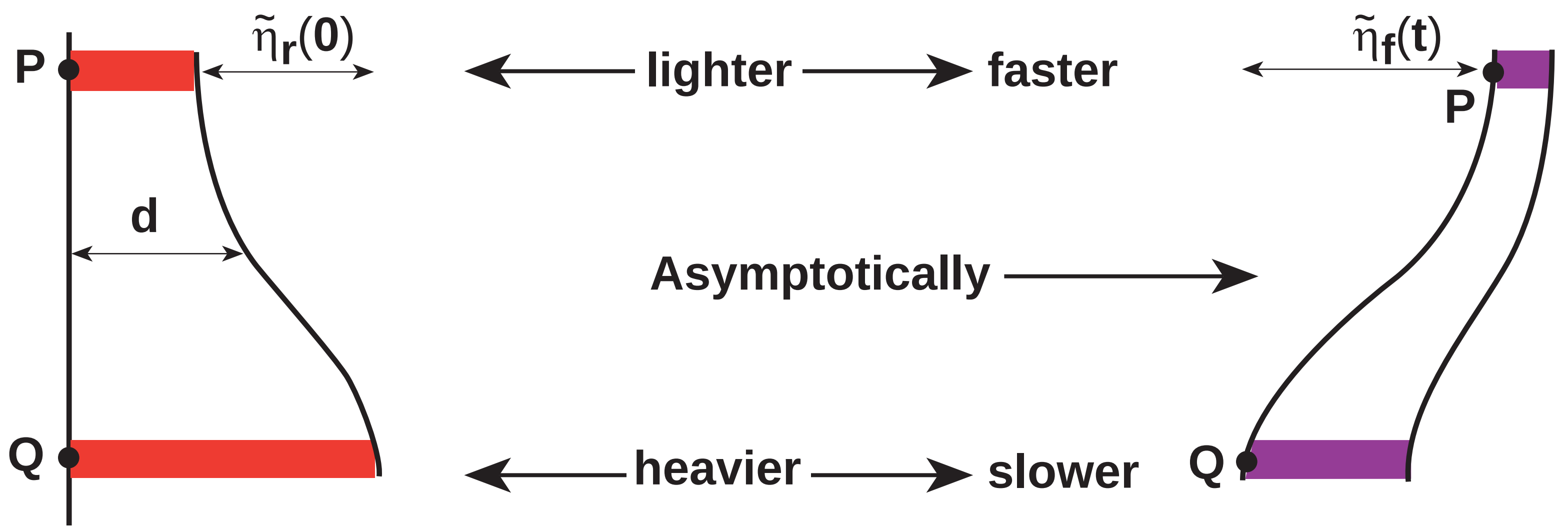

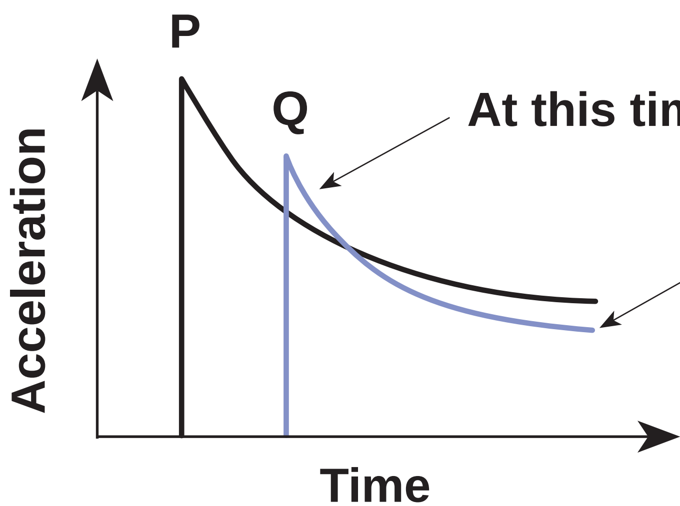

At this time, the acceleration of P is less than Q's.

Later in time, the acceleration of P is greater than Q's.

$$\tilde{g} = g_P - g_Q = -\frac{\partial g}{\partial d}\,\tilde{\eta}_r(0)$$

asymptotic growth $\rightarrow \tilde{\eta}_f(t) \sim \tilde{g}\,t^2/2$

TC4772

The predicted ablation-front-surface ripple-amplitude evolution is in good agreement with the simulation results when the perturbed acceleration is included

Ablation-front-surface distortion versus time

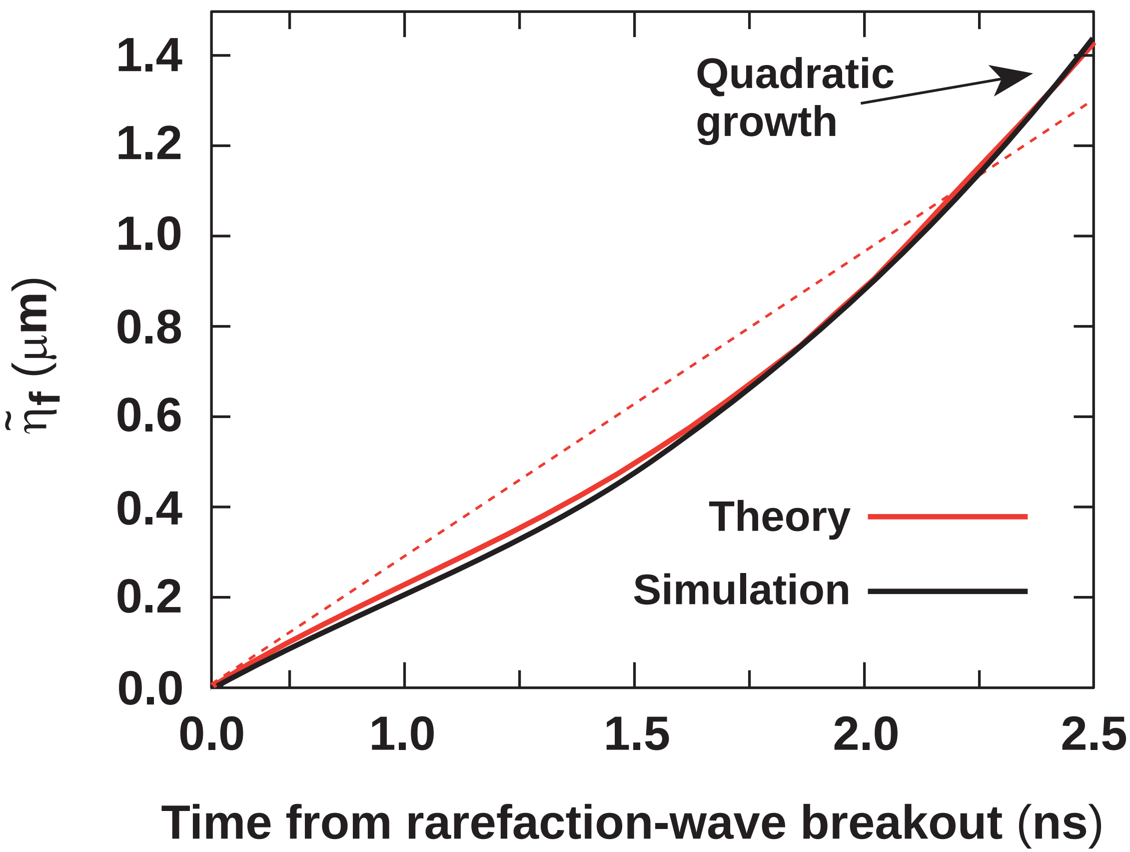

Sharp boundary model

$$\ddot{\tilde{\eta}}_f = \tilde{g} + \sqrt{kg}\,\tilde{\eta}_f$$

$$\tilde{\eta}_f(0) = 0,\ \dot{\tilde{\eta}}_f(0) = \frac{6}{5} C_s \frac{\tilde{\eta}_r(0)}{d_{comp}}$$

TC4775

Both theory and simulations indicate that the transfer function for NIF is well below unity for $\ell > 30$

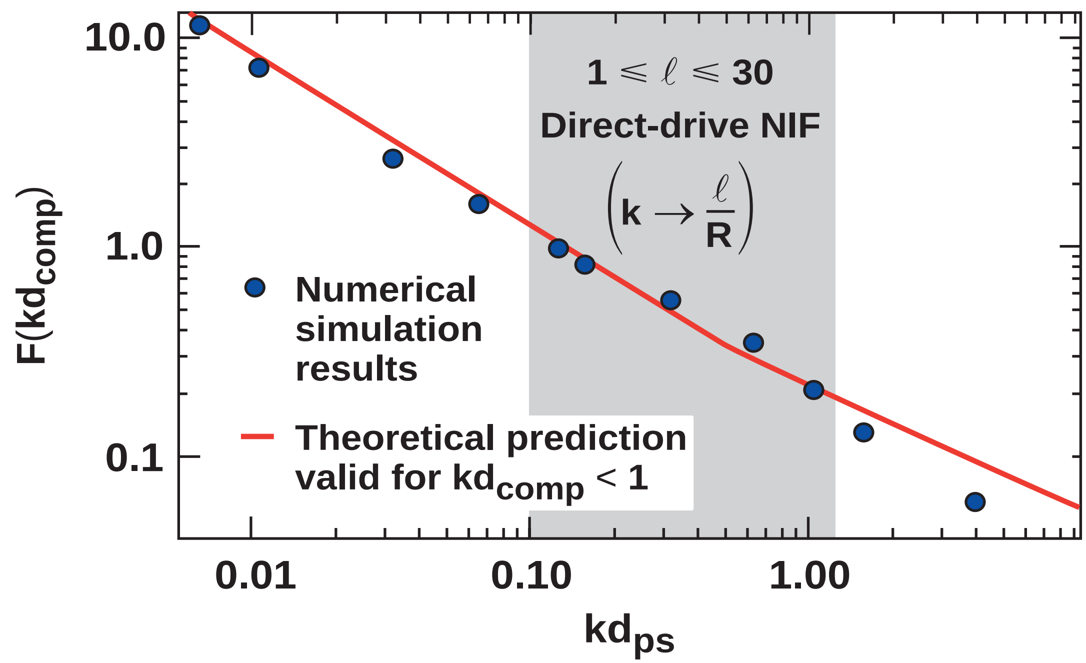

$$\eta_f(t) = \eta_r(0)\, F(kd_{comp}) \exp\left[\int_{t_{rb}}^{t} \sqrt{kg(t')}\,dt'\right]$$

- Transfer function from theory $F(kd_{comp}) = \frac{1}{16}\left[\frac{1}{kd_{comp}} + \frac{2.5}{\sqrt{kd_{comp}}}\right]$

TC5417

Feed-out of the rear-surface perturbation was measured for three wavelengths

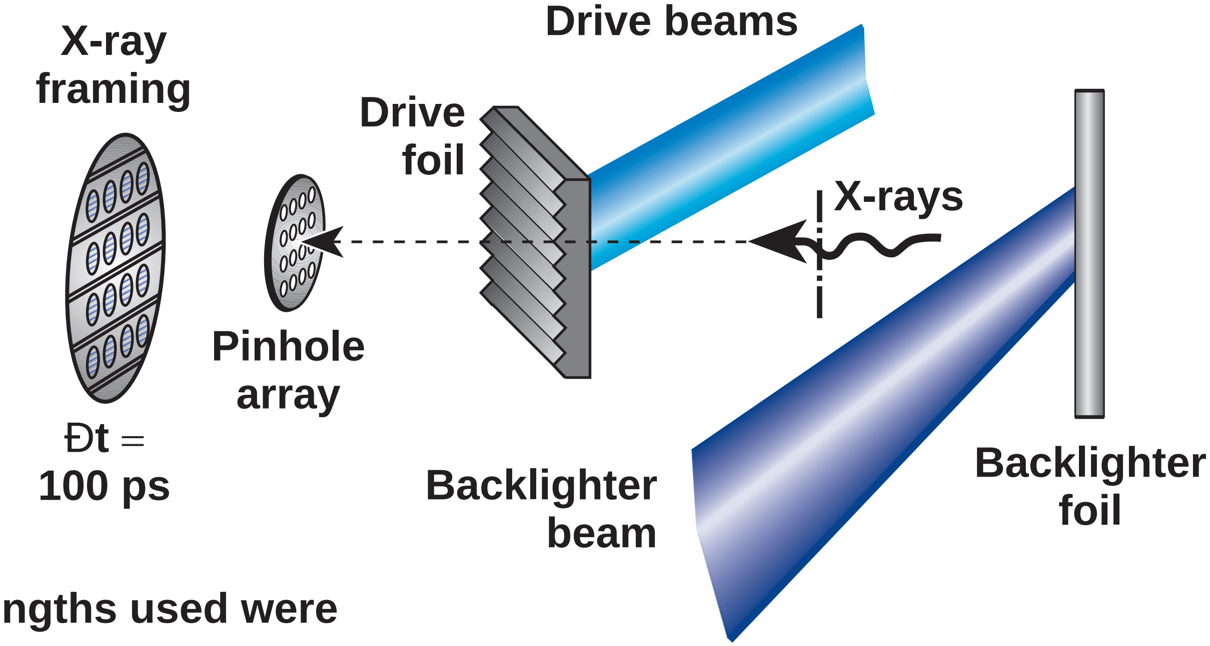

- Perturbation wavelengths used were
  - 60 μm with a 0.5 μm amplitude
  - 30 μm with a 0.5 μm amplitude
  - 20 μm with a 0.5 μm amplitude
- Target foils were constructed from 20-μm-thick CH.
- Targets with 60-μm wavelength perturbations had a front-surface amplitude = 10% of rear-surface amplitude (0.05 μm).

E10125

Calculated ρR from sharp boundary model agrees with experimentally measured optical depth

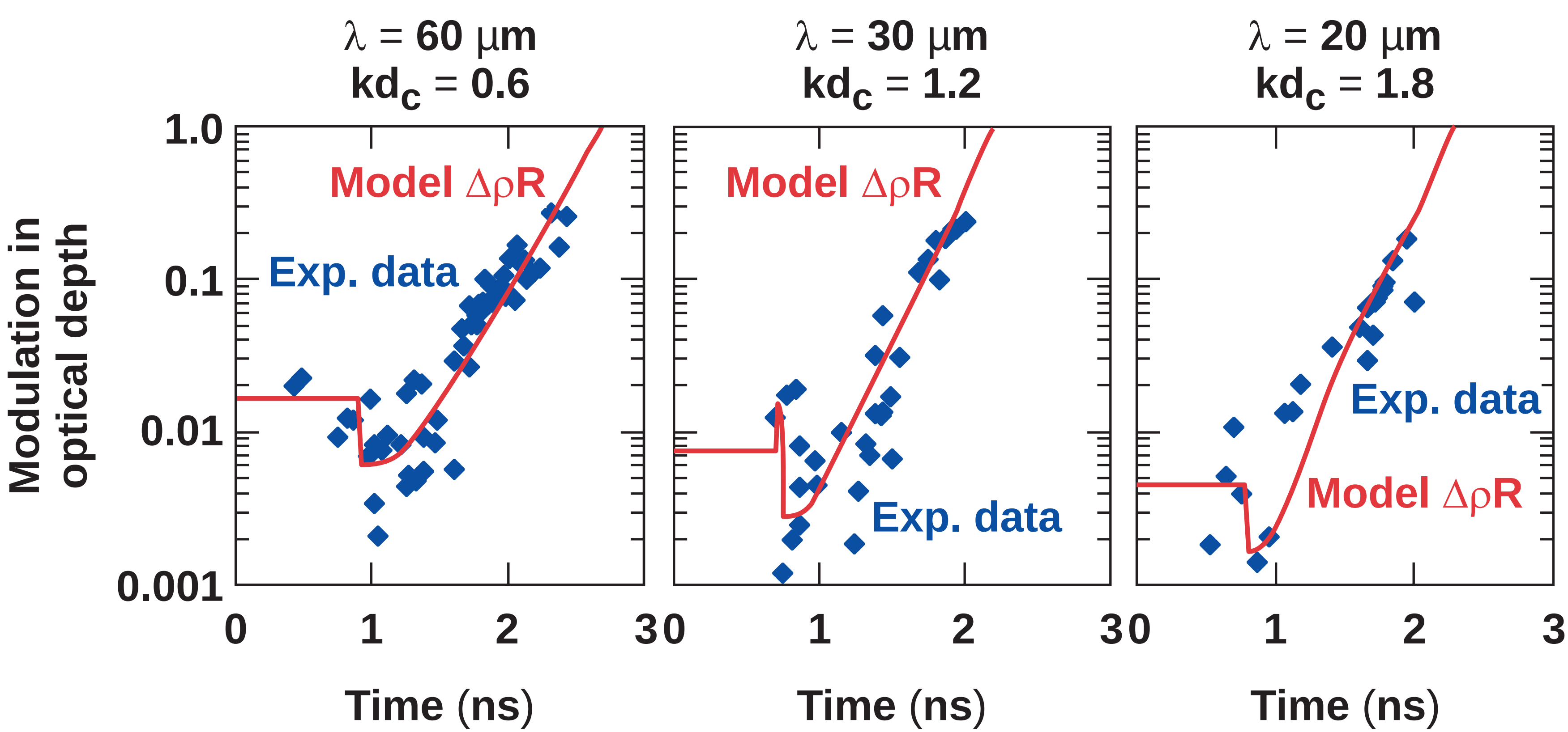

- ρR is scaled by x-ray mfp and framing camera MTF.

E10165a

RT seeding by laser-intensity nonuniformities

UR LLE

Laser Imprintings

Hydrodynamic flow is the main imprint mechanism: velocity perturbation

- Post-shock speed depends on the ablation pressure $U_{ps} \sim \sqrt{p_a}$

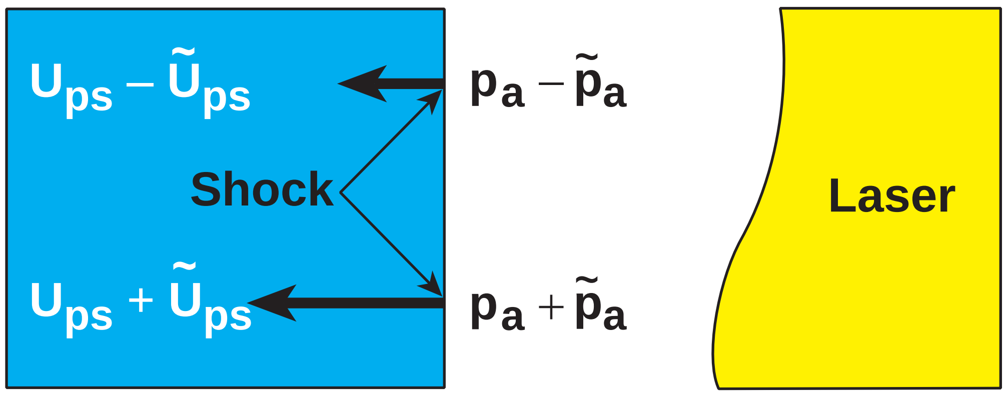

$$\tilde{v} \sim \tilde{U}_{ps} \sim \frac{1}{2} U_{ps} \frac{\tilde{p}_a}{p_a}$$

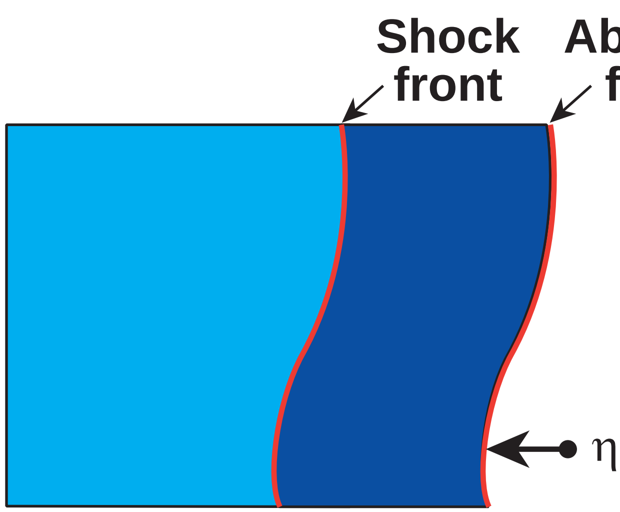

$$\frac{d\tilde{\eta}}{dt} = \tilde{v} \sim U_{ps} \frac{\tilde{p}_a}{p_a}$$

$$\boxed{\tilde{\eta}_{vel} = \tilde{v}t \sim \frac{\tilde{p}_a}{p_a} c_s t}$$

TC5215

Hydrodynamic flow is the main imprint mechanism: acceleration perturbation

- Rippled shock creates lateral mass flow.

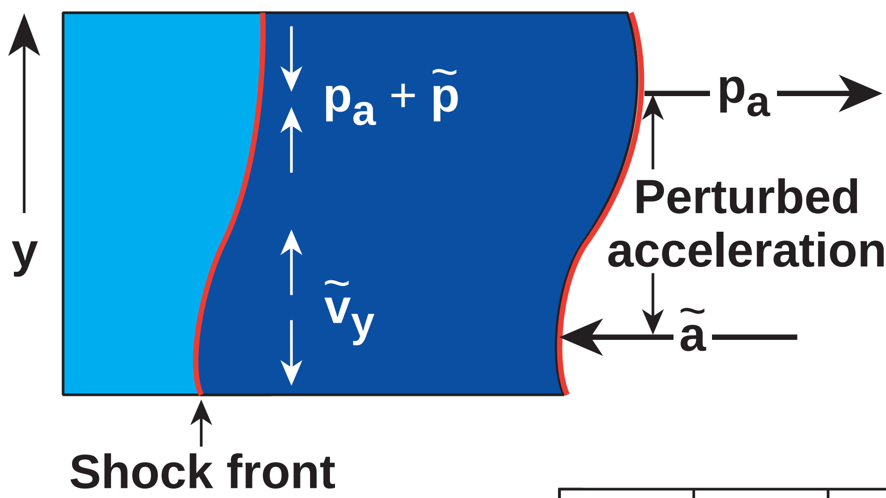

$$\frac{d^2\tilde{\eta}}{dt^2} = \tilde{a} \propto k\frac{\tilde{p}_a}{\rho}$$

$$\boxed{\eta_{ac} \propto k\frac{\tilde{p}_a}{p_a}c_s^2 t^2}$$

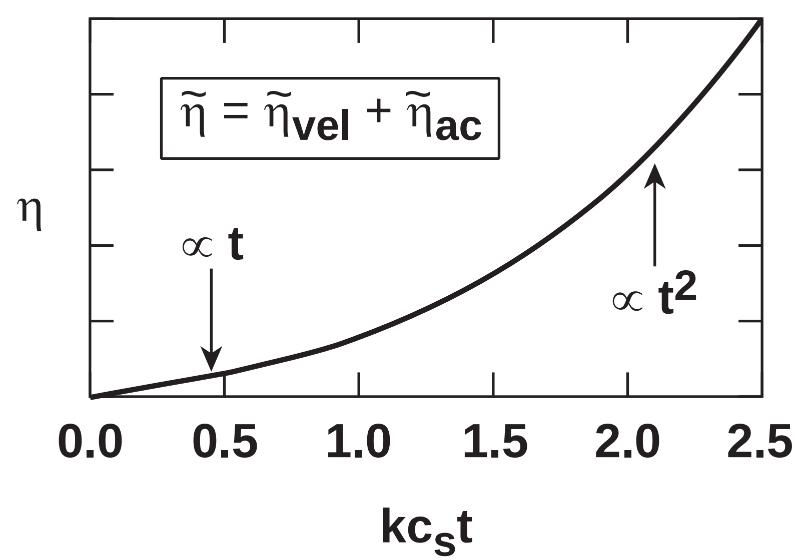

TC5219

Thermal smoothing[1] suppresses acceleration perturbations

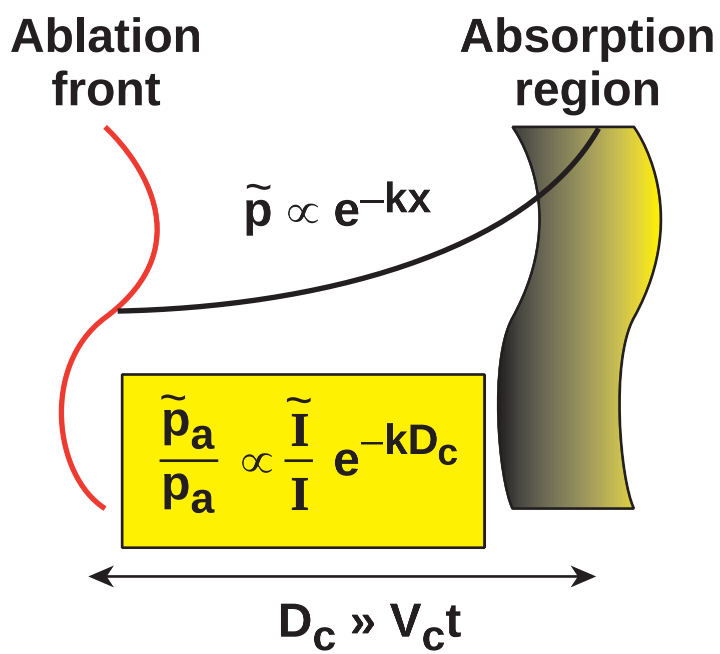

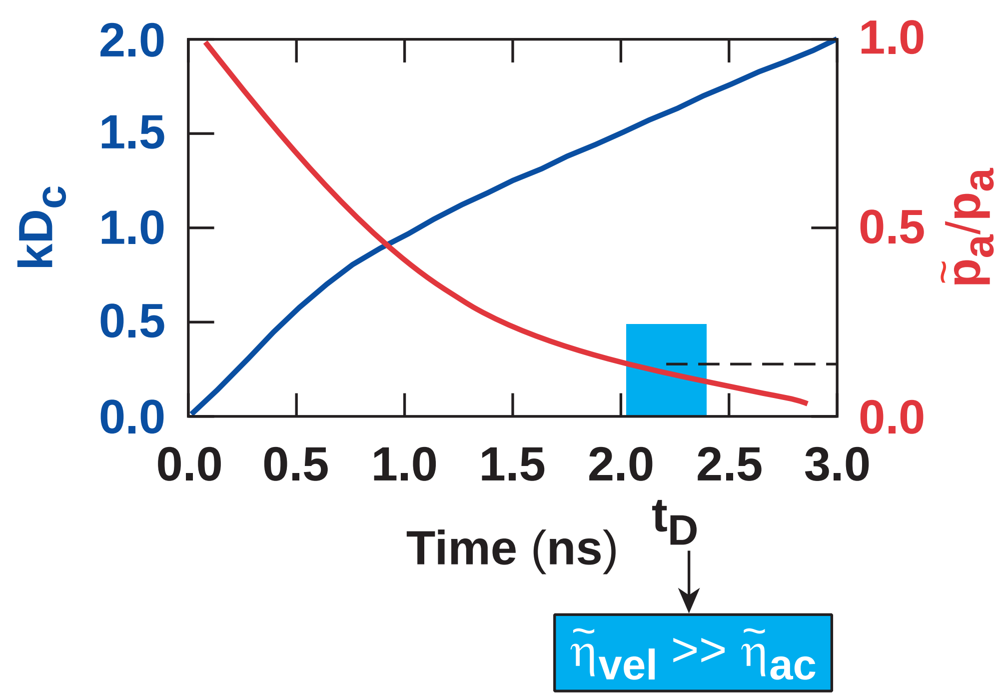

- Laser perturbations decouple from the ablation front when $kD_c \sim 1$.

Decoupling time $t_D \propto (kV_c)^{-1}$

[1]K. A. Brueckner and S. Jorna, Rev. Mod. Phys. 46, 325 (1974).

TC5274

Imprint growth is reduced by thermal smoothing

- After decoupling time $t > t_D$, $\tilde{a} = 0$.

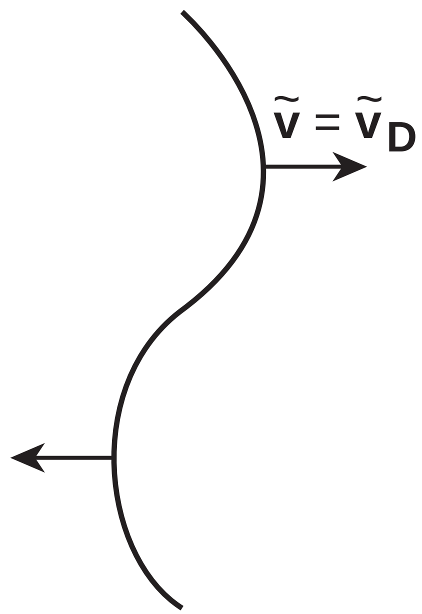

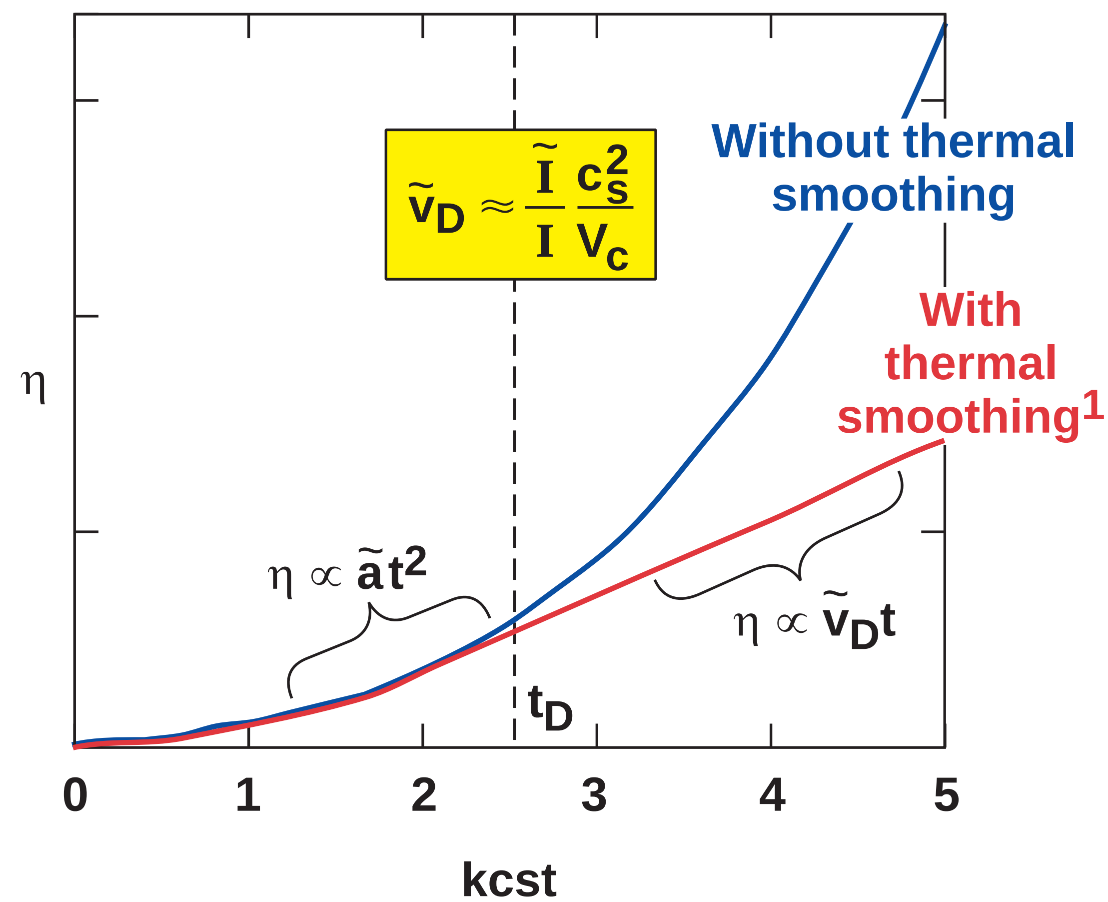

[1]A. Velikovich *et al.*, Phys. Plasmas 5, 1491 (1998).

TC5275

The most damaging modes oscillate during the shock propagation

- Single-mode imprint *ORCHID* simulations

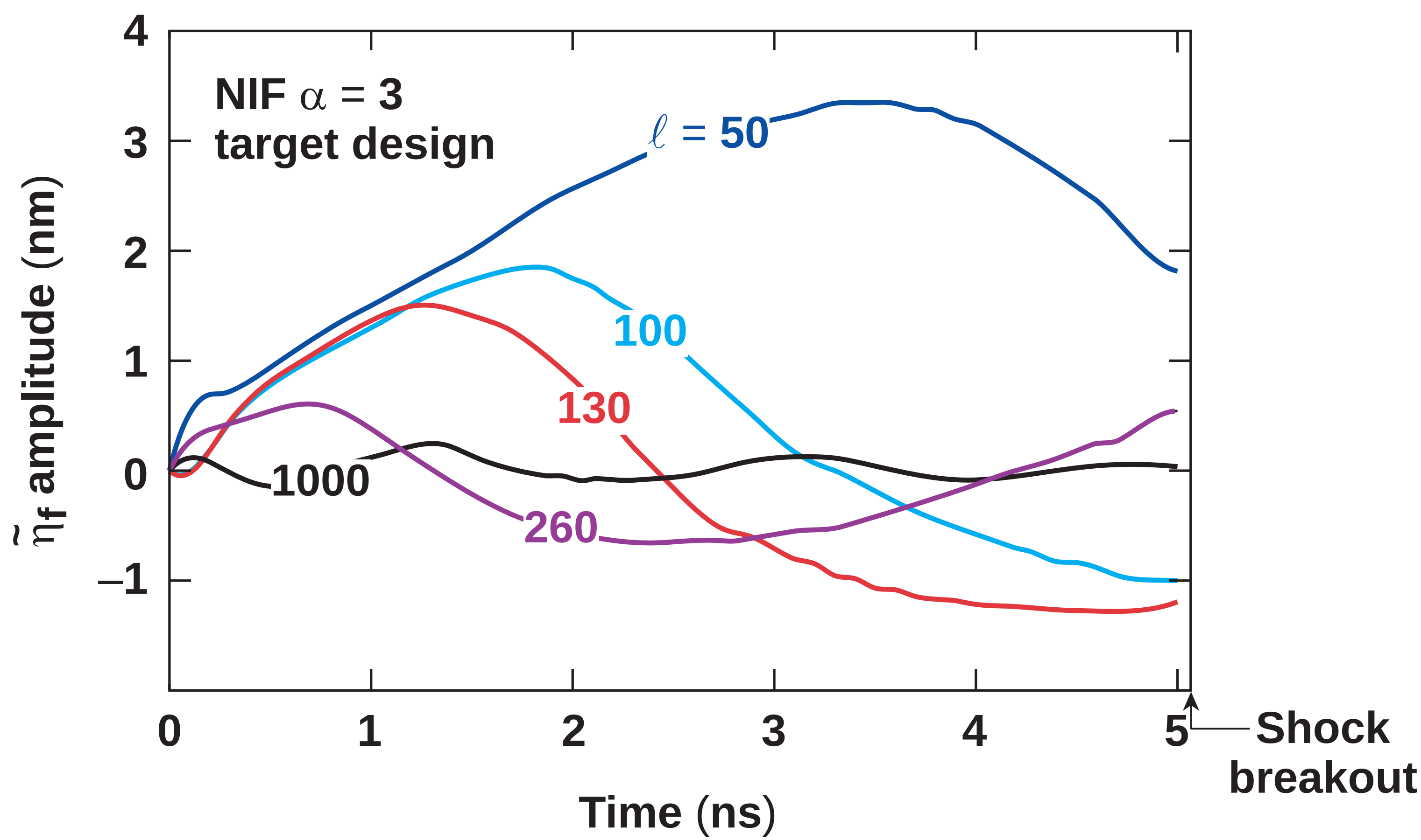

TC5270

Mode spectrum at the beginning of the acceleration phase is used as an initial condition for RT postprocessor

- Initial conditions for RT model

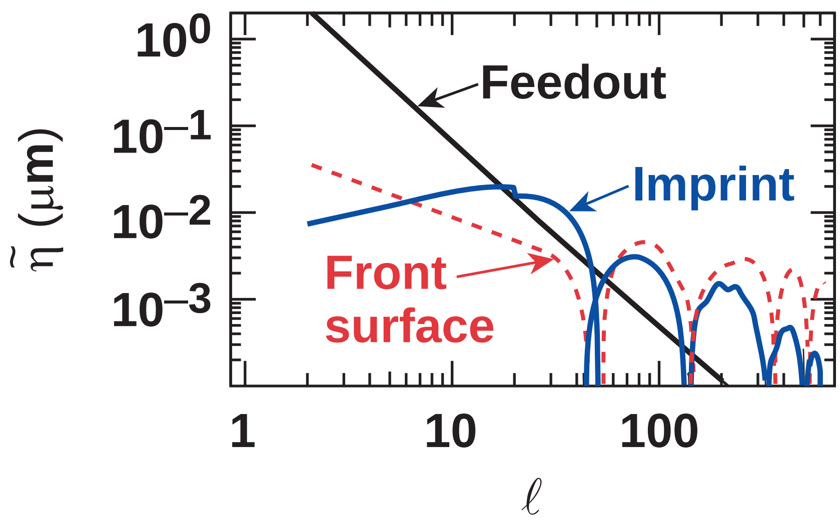

- RT postprocessor

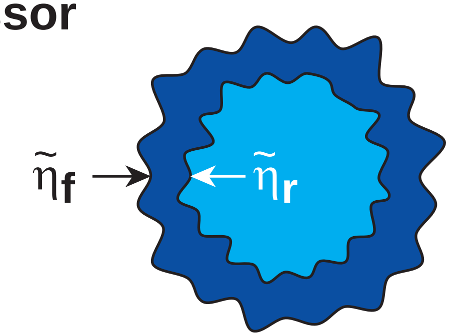

$$\begin{cases} \sum_{j=0}^{2}\left[C_j \frac{d^j}{dt^j}\eta_f + D_j \frac{d^j}{dt^j}\eta_r\right] = 0 \\ \sum_{j=0}^{2}\left[E_j \frac{d^j}{dt^j}\eta_f + F_j \frac{d^j}{dt^j}\eta_r\right] = 0 \end{cases}$$

TC5133a

The results of the model are in good agreement with multimode *ORCHID* simulations

- Multimode perturbation at the beginning of the deceleration phase.

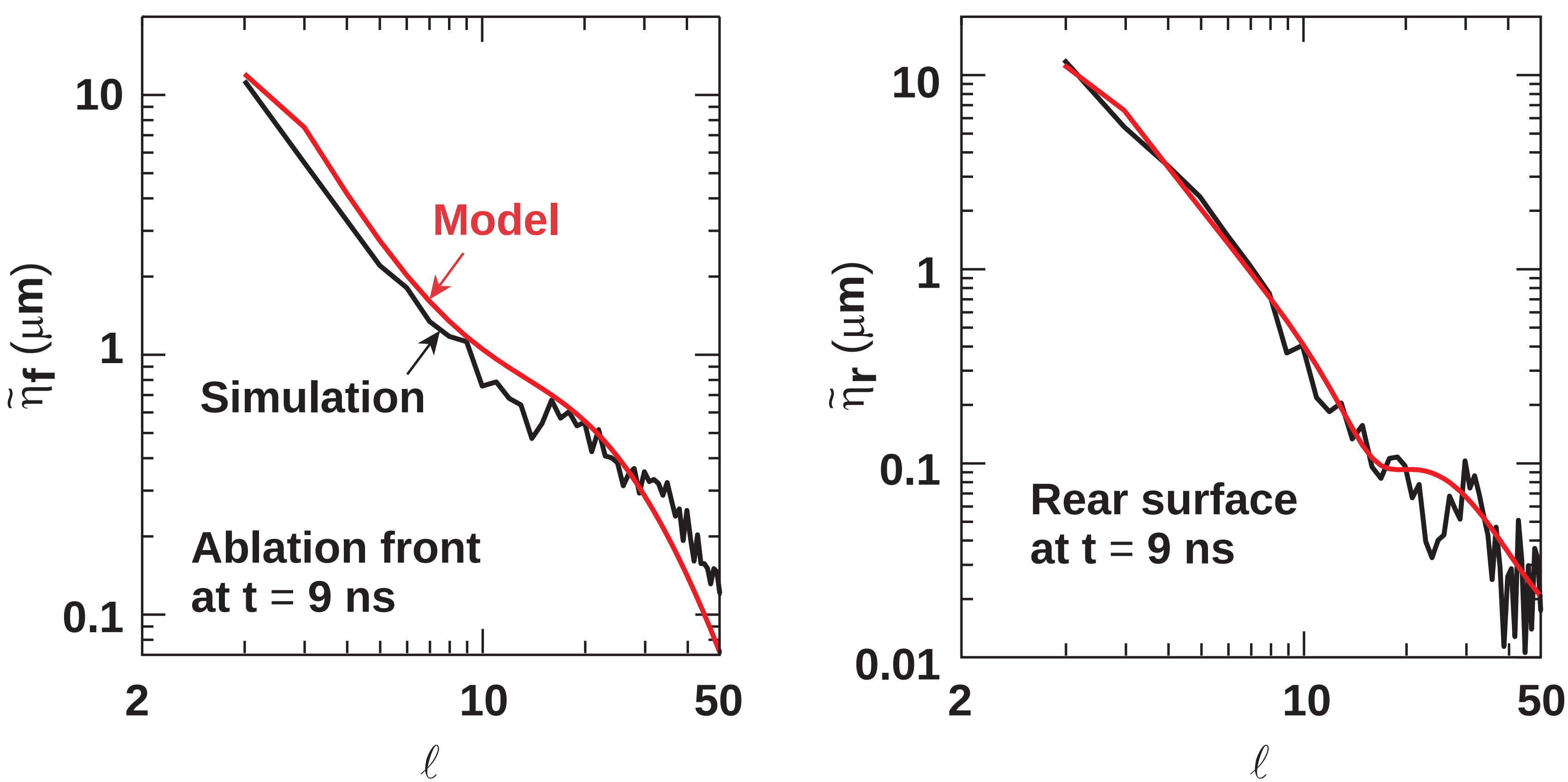

TC5389

Deceleration phase instabilities

- The simple model of a decelerating foil
- The seeds
- The growth rates
- Change of motation:
  ablation front $\rightarrow$ outer surface
  rear surface $\rightarrow$ inner surface.

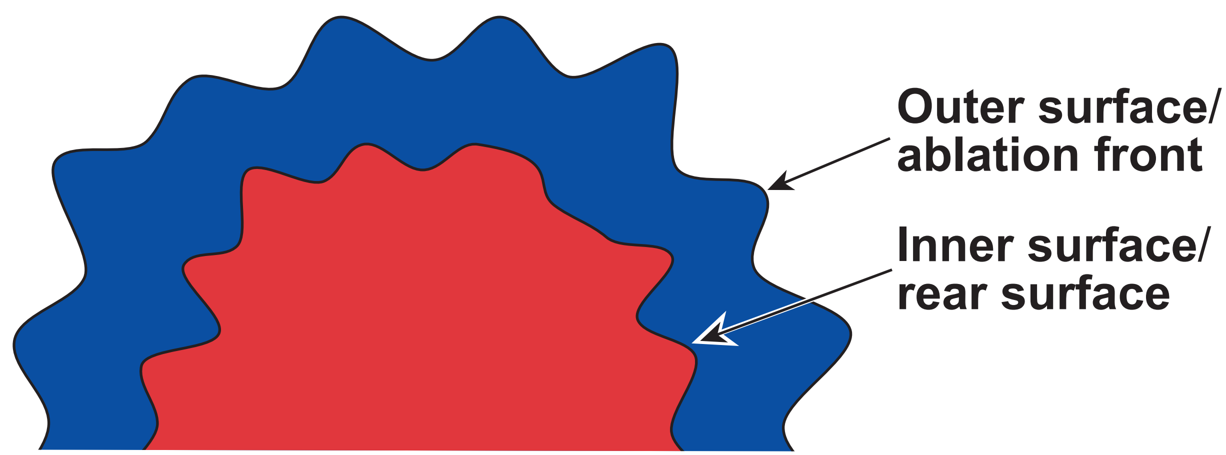

TC5390

The decelerating foil problem provides the basic understanding of the deceleration-phase instability

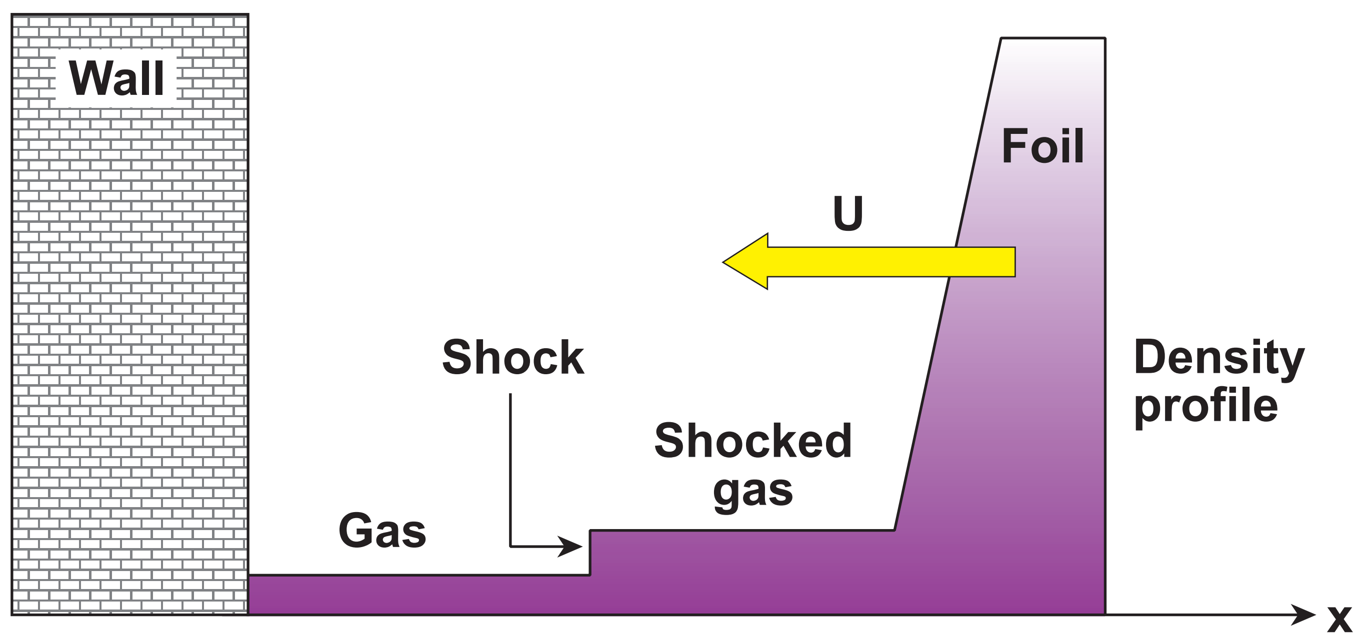

- The shock reflected from the wall slows down the foil, which in turn compresses the gas and decelerates.
- The 1-D problem can be solved analytically leading to a clear understanding of the relevant physics issues.

The foil is slowed down both impulsively and continuously

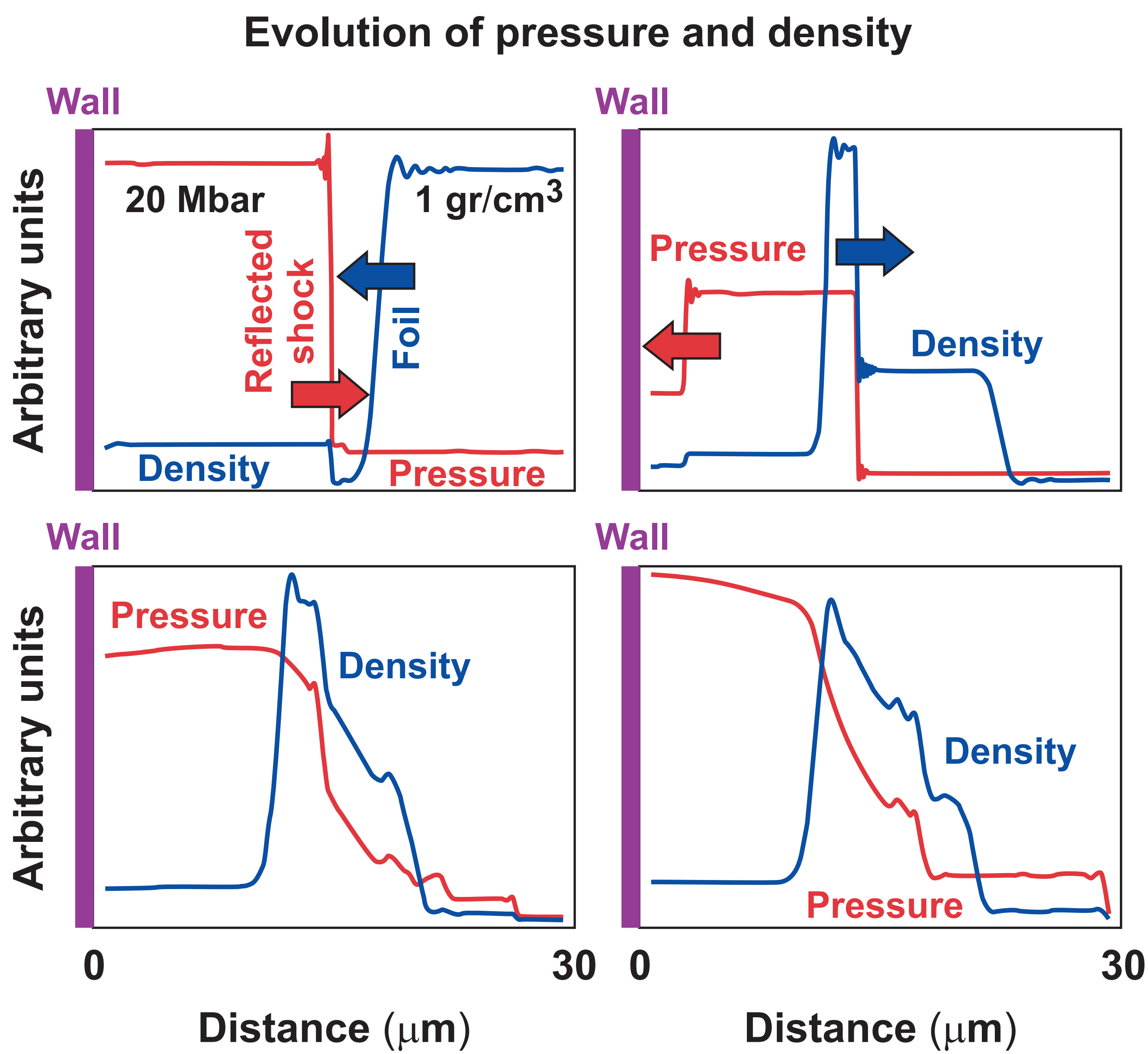

TC5392

Dec. RT seeding by outer-surface nonuniformities

FEEDTHROUGH

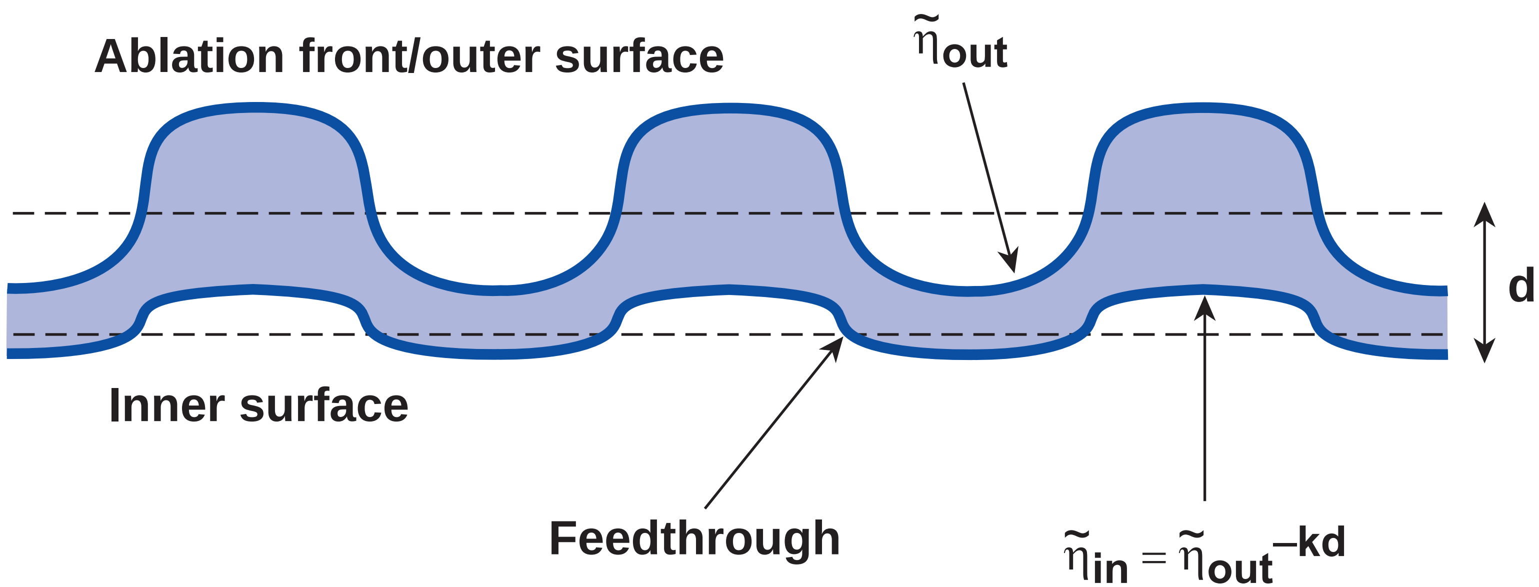

TC5399

As expected, the foil inner surface is hydrodynamically unstable

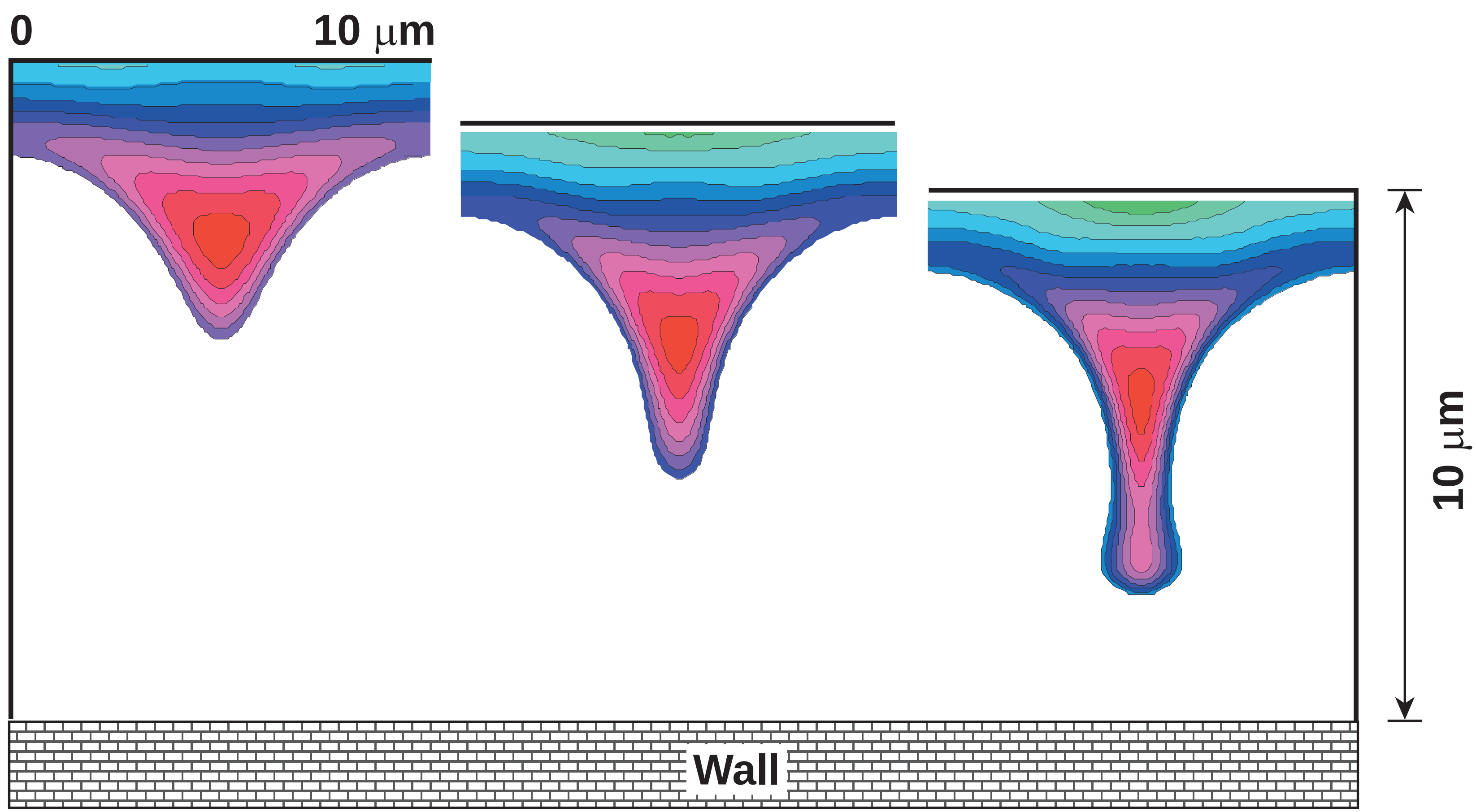

TC5400

The deceleration-phase instability is a combination of Richtmyer–Meshkov and Rayleigh–Taylor

Linear growth of a 10-μm-wavelength perturbation

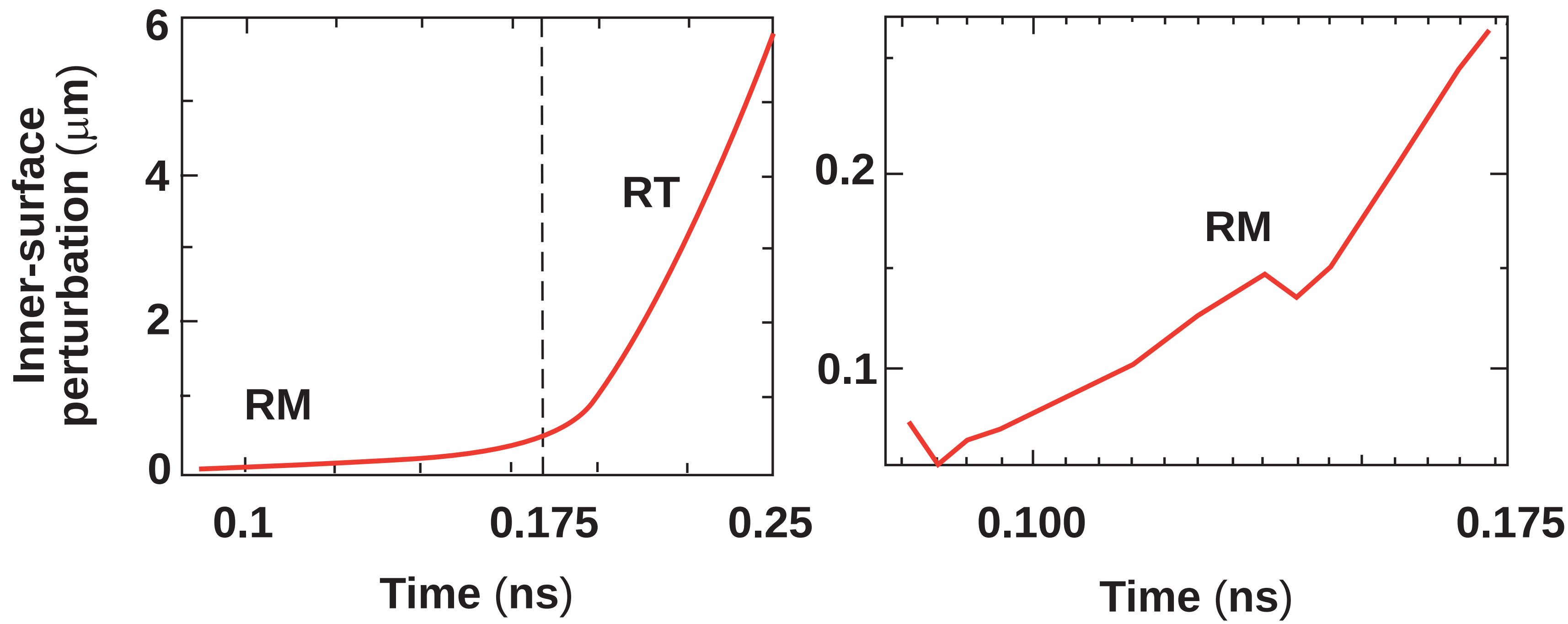

TC5401

Dec. RT seeding by outer-surface nonuniformities

UR LLE

Reverse Feedout

Reverse feedout is also a RT seed during the deceleration phase

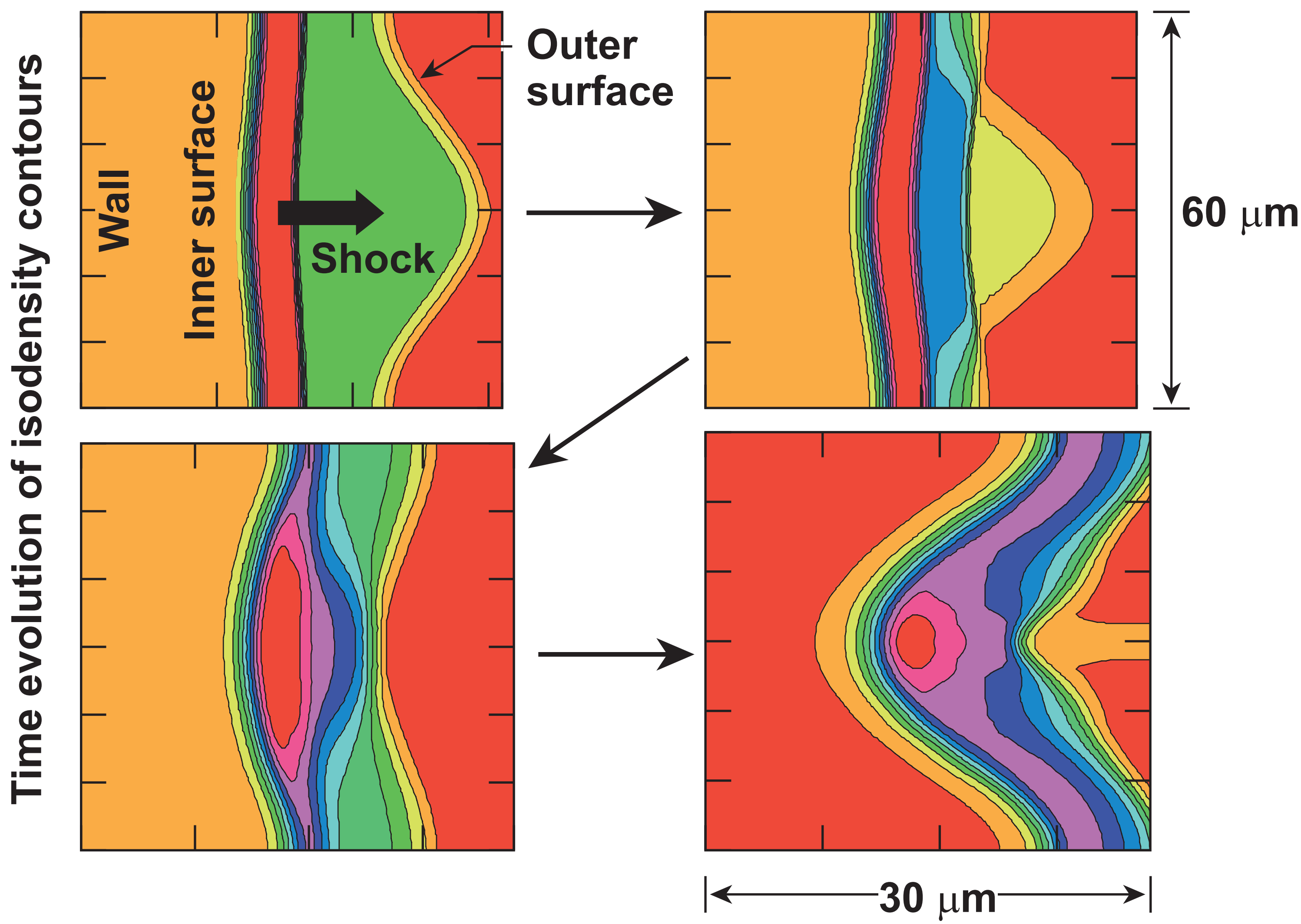

TC5403

The outer surface perturbations seed the deceleration RT

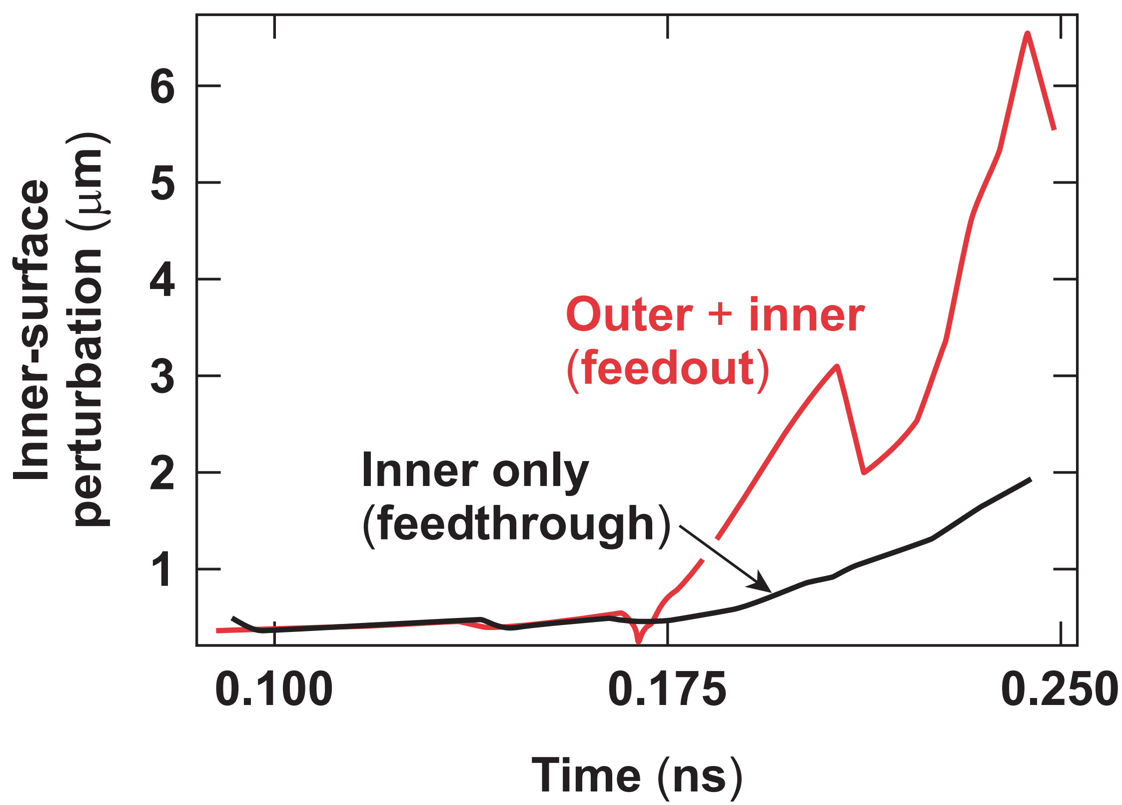

- The feedout is back!

TC5404

Deceleration phase RT instability

The Growth Rates

Not much is known about the RT growth rates during the deceleration phase

- The only mention of deceleration-phase RT growth rates is in Lindl's book:

$$\gamma_{cl} = \left[\frac{kg}{1 + kL}\right]^{1/2}$$

- Lindl's estimate for spherical implosions is $L \sim 0.2\ R_{hot\ spot}$.
- For NIF, $R_{hot\ spot} \sim 50$ to $100\ \mu m \rightarrow L \sim 10$ to $20\ \mu m$.
- Such a large L has a strong stabilizing effect.

J. D. Lindl, "Inertial Confinment Fusion" (AIP Press, 1998).

The heat flux leaving the hot-spot is deposited on the shell surface causing mass ablation from the shell into the hot spot. The hot-spot mass increases in time

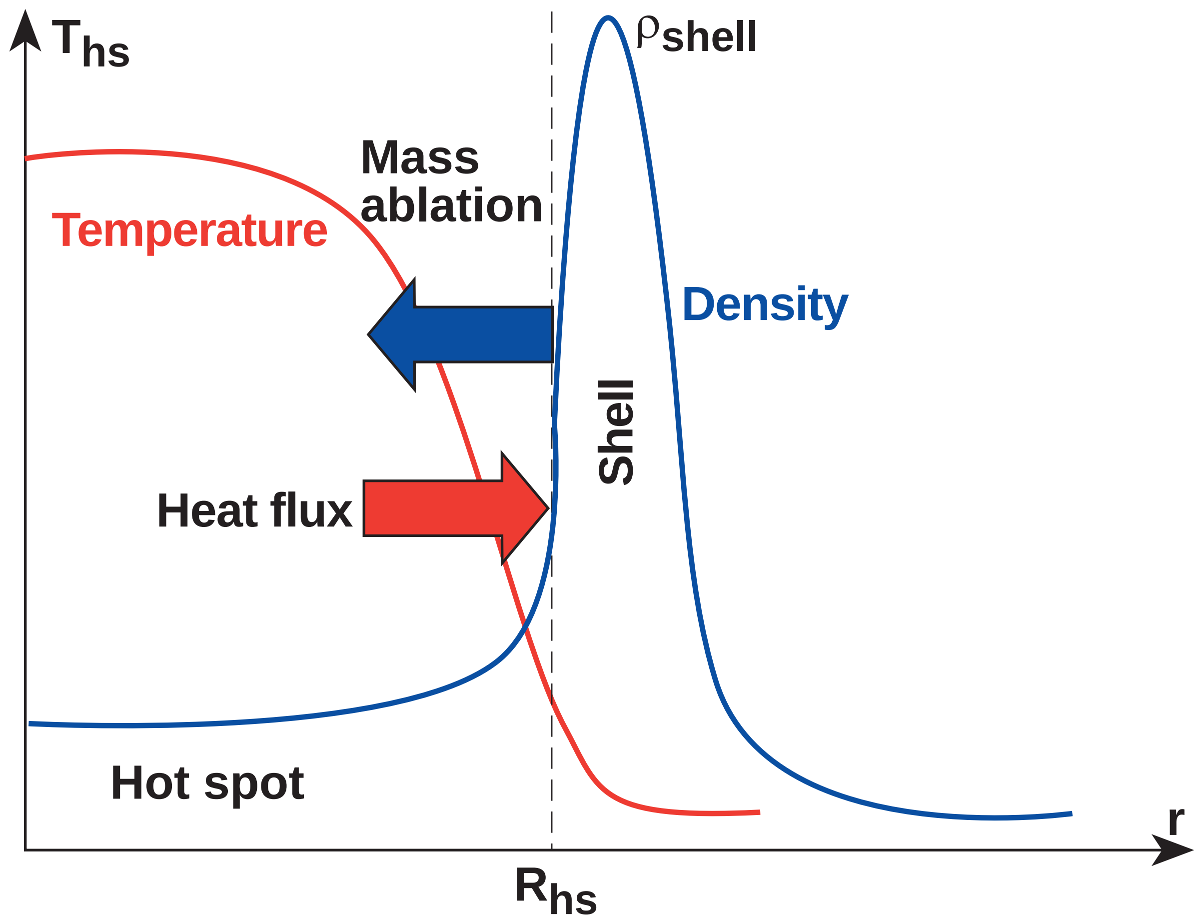

TC5407

The ablation velocity is determined from the energy balance

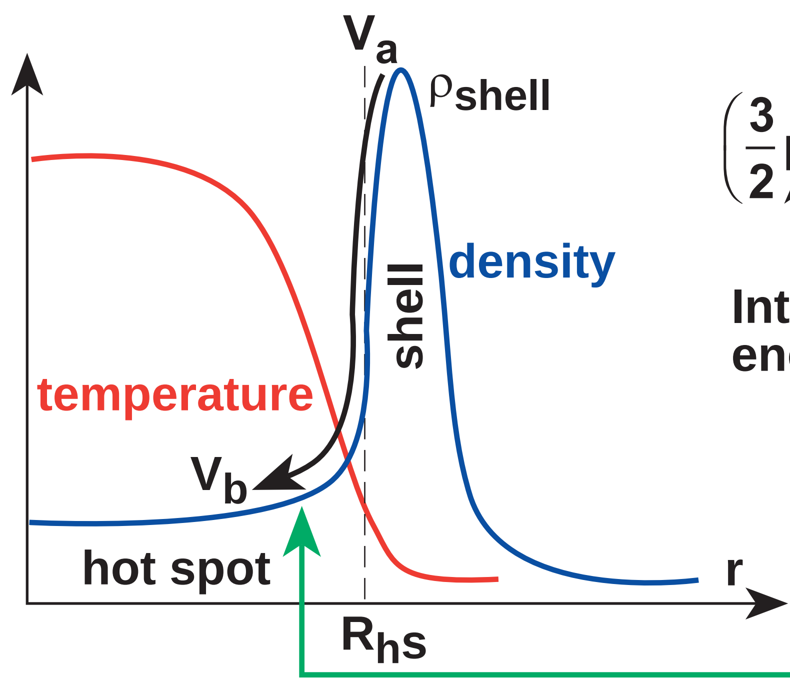

$$\left(\frac{3}{2}p_b V_b + p_b V_b\right) = \kappa_{Spitz}(T_b)\frac{dT_b}{dR_{hs}}$$

Internal energy flux

pdV work rate

Energy flux balance

- Hot-spot temperature profile: $T_{hs} = T_0\left(1 - \frac{r^2}{R_{hs}^2}\right)^{2/5}$
- Use the EOS: $p_b V_b = 2\rho_b V_b T_b / M_i = 2\dot{m} T_b / M_i$
- Ablation velocity: $V_a = \frac{\dot{m}}{\rho_{shell}} = 0.2\frac{M_i \kappa_{Spitz}(T_0)}{\rho_{shell} R_{hot\ spot}}$

TC5408

The density-gradient scale length is small

- Balance of heat flux to the shell and internal energy flux leaving the shell

$$pV_a \approx -\kappa\left(T_{sh}\right)\frac{dT_{sh}}{dr} \approx \kappa\left(T_{sh}\right)T_{sh}\,\frac{1}{\rho_{sh}}\frac{d\rho_{sh}}{dr}$$

- The density-gradient scale length is found using the formula for the ablation velocity:

$$L_m = \left[\frac{1}{\rho}\frac{d\rho}{dr}\right]_{min}^{-1} \approx 1.6\,\frac{M_i\kappa\left(T_{sh}\right)}{\rho_{sh}V_a} = 8R_{hot\text{-}spot}\left(\frac{T_{shell}}{T_0}\right)^{5/2}$$

- For NIF: $L_m \sim 1\ \mu m$

TC5409

Planar simulations reproduce the behavior of ICF capsule implosions

- Hot-spot temperature and radius and peak shell density have the same order of magnitude in planar and spherical cases.

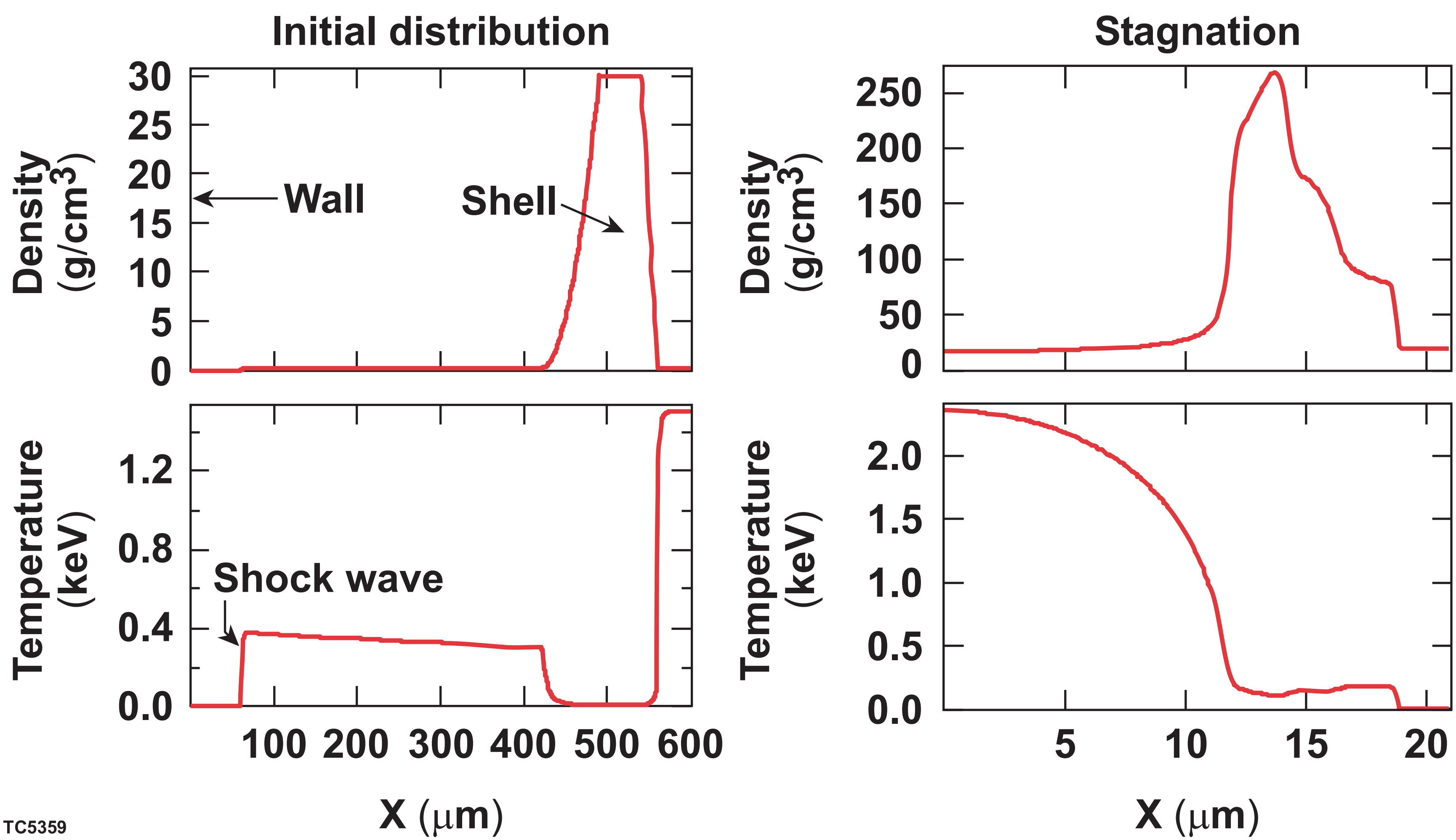

TC5359

Ablation velocity is significant during the deceleration phase

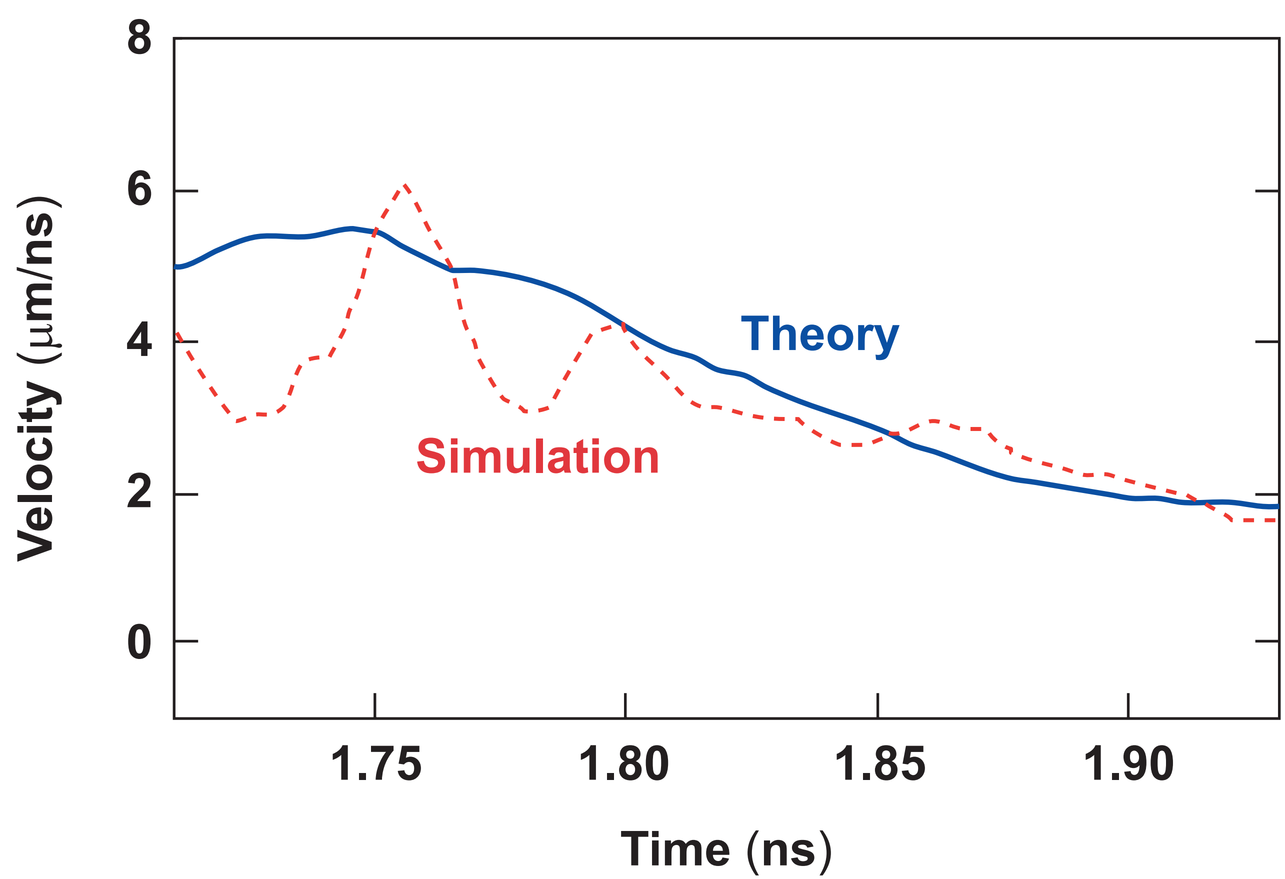

TC5362a

A significant reduction in RT growth rates is due to ablation

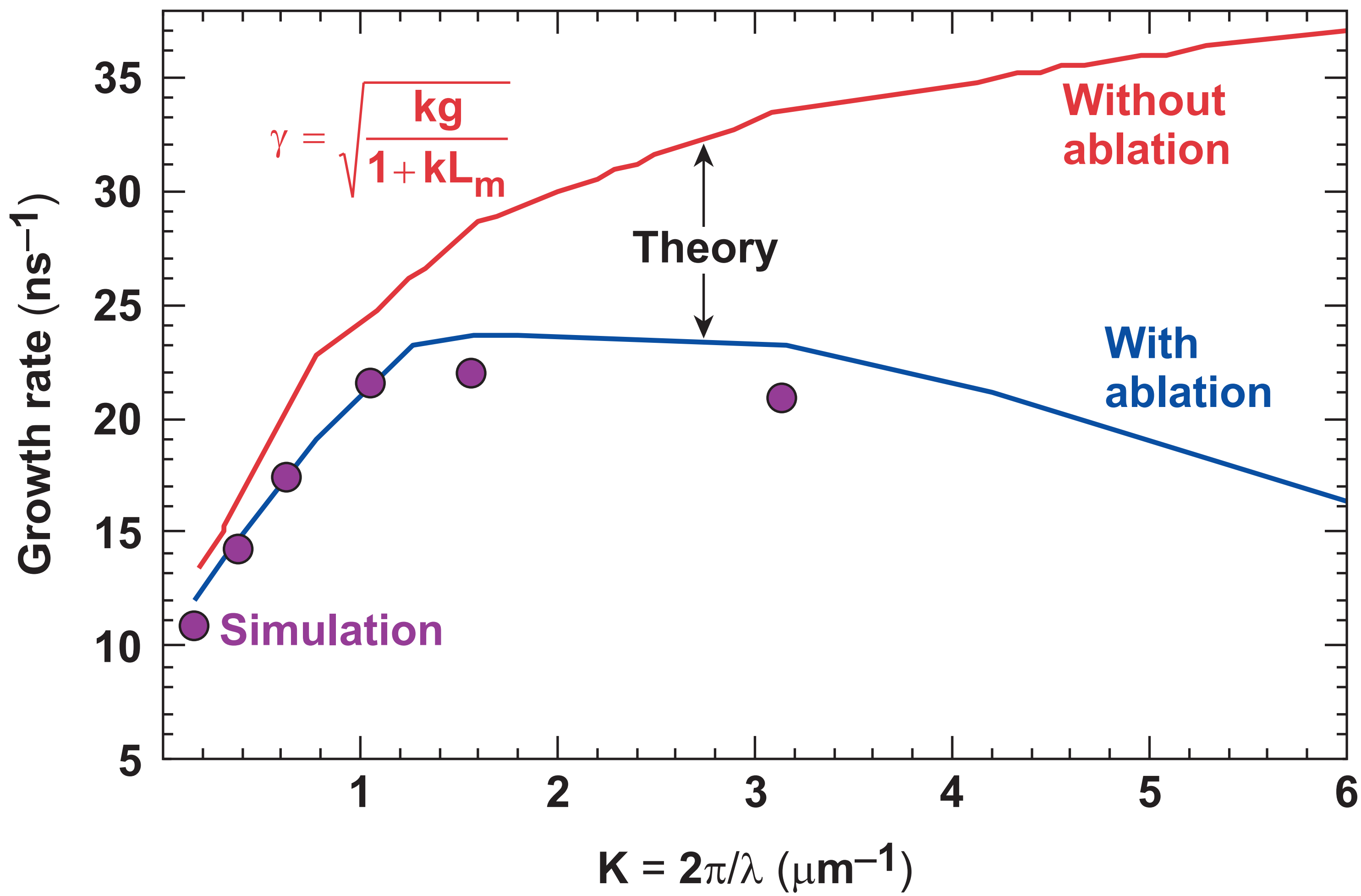

TC5366

Theory and 1-D *LILAC* simulations yield the same value of the ablation velocity

UR LLE

Time 10.40 ns

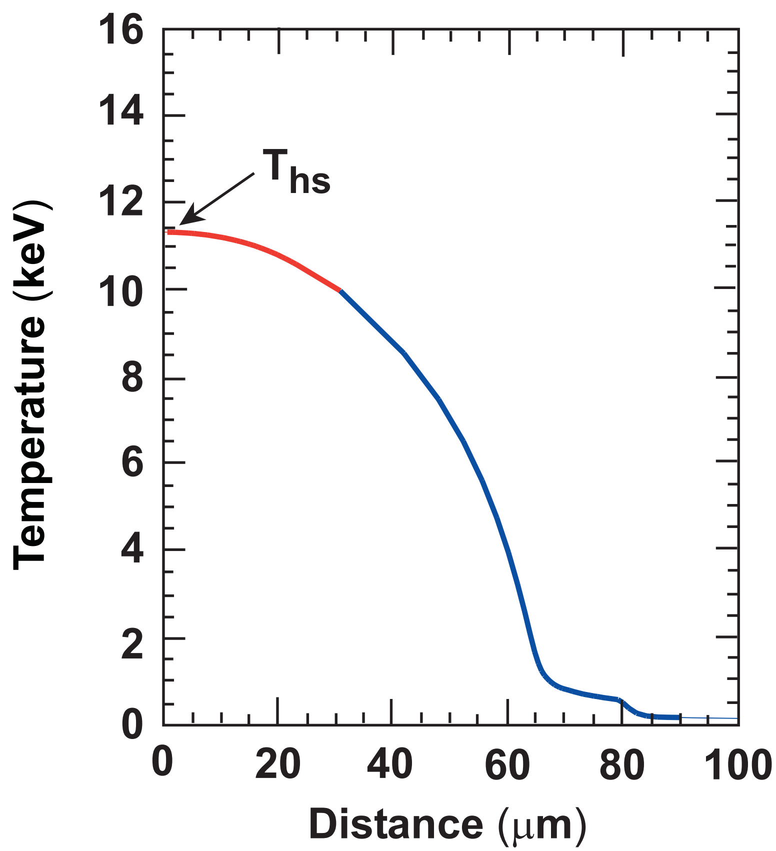

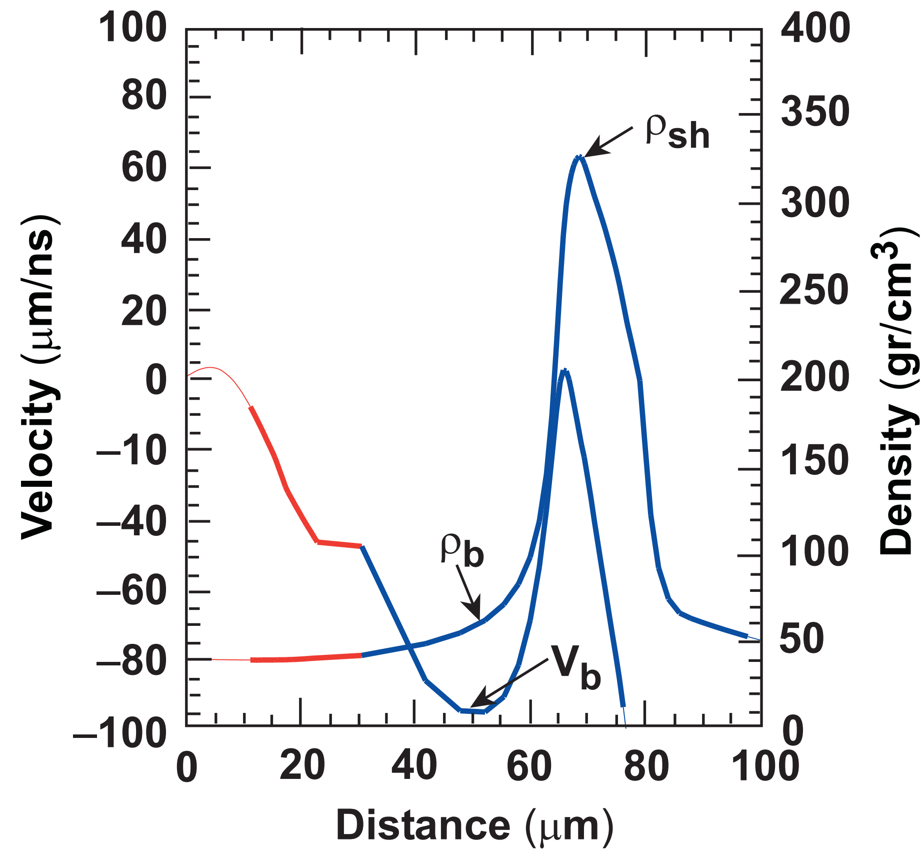

- From theory using T_{hs} = 11.5 keV, ρ_{sh} = 325 gr/cm^3, R_{hs} = 65 μm → V_a = 25 μm/ns
- From simulations: V_b = 100 μm/ns, ρ_b = 60 gr/cm^3, $V_a = \rho_b$; V_b/ρ_{sh} = 20 μm/ns

TC5410

Theoretical NIF linear growth factors are significantly reduced by mass ablation

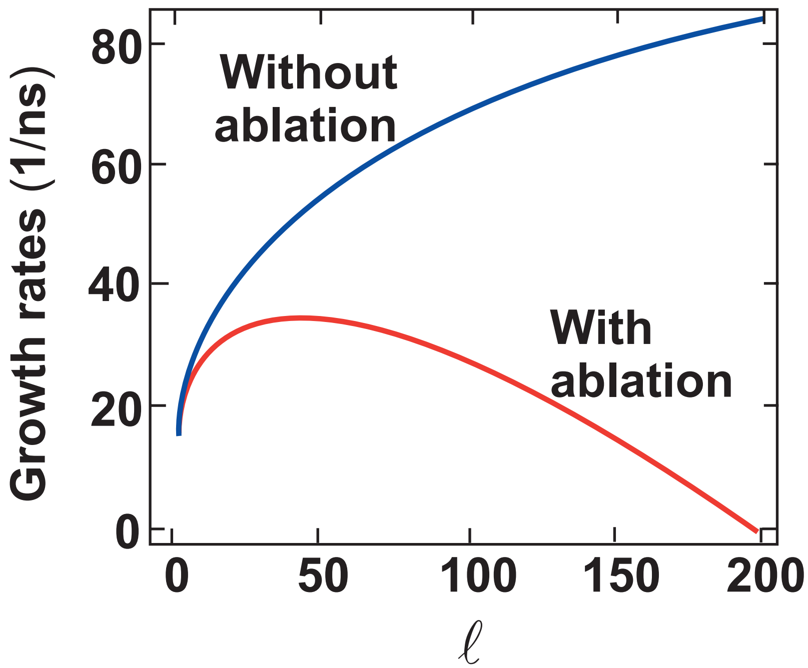

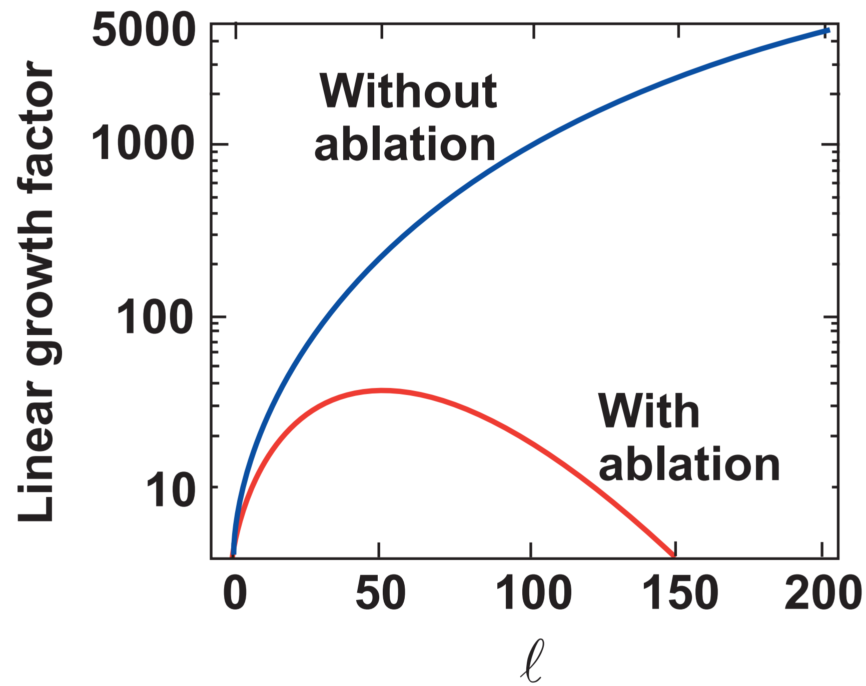

- Growth rate formula from R. Betti, *et al.*, Phys. Plasma 1998.
- NIF deceleration phase: $g = 10^4\ \mu m/ns^2$, $V_a = 20\ \mu m/ns$, $R_{hs} = 70\ \mu m$, $L_m = 1\ \mu m$.
- Duration of deceleration phase ~ 100 ps.

NIF cutoff: $\ell \approx 190$

TC5411

Conclusions

- **Two stages of the deceleration-phase instability are observed: deceleration by a series of shocks and continuous deceleration.**
- **Mass ablation through the inner surface and finite density-gradient scale length are the most important stabilizing effects.**
- **A significant reduction in the RT instability growth rate is due to the mass ablation.**
- **The inner-surface density-gradient scale length is lower than its standard estimate (~0.2 hot-spot radius).**
- **The cutoff wave number of the deceleration-phase RT for NIF is approximately ℓ_{cutoff} = 150 to 200.**